batteries

MDPI

Review

Current Advances in TiO_2-Based Nanostructure Electrodes for High Performance Lithium Ion Batteries

Mahmoud Madian [1,2,*], Alexander Eychmüller [3] and Lars Giebeler [1]

1 Leibniz-Institute for Solid State and Materials Research (IFW) Dresden e.V., Institute for Complex Materials, Helmholtzstr. 20, D-01069 Dresden, Germany; l.giebeler@ifw-dresden.de
2 Physical Chemistry Department, National Research Centre, 33 El-Buhouth St., Dokki EG-12622, Giza, Egypt
3 Physical Chemistry Department, Technische Universität Dresden, Bergstr. 66b, D-01069 Dresden, Germany; alexander.eychmueller@chemie.tu-dresden.de
* Correspondence: m.madian@ifw-dresden.de

Received: 20 November 2017; Accepted: 20 January 2018; Published: 6 February 2018

Abstract: The lithium ion battery (LIB) has proven to be a very reliably used system to store electrical energy, for either mobile or stationary applications. Among others, TiO_2-based anodes are the most attractive candidates for building safe and durable lithium ion batteries with high energy density. A variety of TiO_2 nanostructures has been thoroughly investigated as anodes in LIBs, e.g., nanoparticles, nanorods, nanoneedles, nanowires, and nanotubes discussed either in their pure form or in composites. In this review, we present the recent developments and breakthroughs demonstrated to synthesize safe, high power, and low cost nanostructured titania-based anodes. The reader is provided with an in-depth review of well-oriented TiO_2-based nanotubes fabricated by anodic oxidation. Other strategies for modification of TiO_2-based anodes with other elements or materials are also highlighted in this report.

Keywords: battery; anode; titania; anodic oxidation; composite materials; carbon; performance effect; mixed oxides

1. Introduction

Lithium ion batteries indisputably have become the first choice as primary power sources for portable devices and electric vehicles. They offer valuable properties, i.e., long cycle life, high energy density, reasonable production cost, and the ease of manufacturing flexible designs. These properties are the main reasons behind populating lithium ion batteries as the main part in portable devices, and, in addition, to play a central role in the on-going miniaturization of electronics and medical devices. Indeed, developing anode materials for lithium ion batteries with higher performance and competitive price is still the main hurdle to reduce weight and improve performance of LIBs. Early in 1991, Sony introduced the first lithium ion battery to the market in which graphite was used as active anode material, owing to its abundance, low production cost, and reasonable theoretical capacity (372 mAh g^{-1}) [1–3]. This important event aroused the attention of many researchers and motivated them to do extensive work to improve the performance of lithium ion batteries. However, using graphite as anode material is accompanied by several drawbacks. It suffers from severe structure collapse and exfoliation over cycling that originally starts with the formation of solid electrolyte interface (SEI) followed by rapid capacity fading. The low operating voltage of ~0.1 V vs. Li/Li^+ represents another problem. Such a low potential allows for lithium electroplating at the electrode surface which requires implementing extra materials in the sense of carbon or other materials for safety issues [4]. At a high charging/discharging current rate, lithium dendrites can

easily be formed on the graphite surface due to its high polarization [5]. Such dendrites can move through the separator resulting in an internal short circuit, cell damaging, and warming up until fire (thermal runaway) [6]. Moreover, the use of a graphite-based anode is particularly restricted to low temperatures [7,8]. However, the hybrid electric vehicles (HEVs) and electric vehicles (EVs) are usually charged/discharged at high current rates over a wide temperature range (−30 to +60 °C), where the application of graphite is not suitable and does not meet the EVs requirements. Especially at low temperatures the Li dendrite formation is even enhanced [9]. Therefore, replacing graphite with another material becomes an urgent need. A variety of materials have been proposed as promising candidates for the negative electrode in lithium ion batteries including lithium-metal alloys (Li_xM where, M = Sn [10], Al [11], Ga [12], Ge [13], Pb [14], Sb [15], etc.), silicon-based materials (Si nanostructures, Si/C [16], Cu-Si-Al_2O_3 [17], Ni_3Si_2/Si [18], etc.), layered metal dichalcogenides (MS_2, M = Mo, W, Ga, Nb, and Ta) and transition metal oxides (MO, M = Ti, Sn, etc.) [19]. Figure 1 shows the maximum reversible capacities obtained by some anode materials [20–22]. Although the TiO_2 anode shows a relatively low reversible capacity compared to other transition oxides, it exhibits superior cycling stability and Coulombic efficiency. Additionally, they are abundant, environmentally friendly, and obtained by cost-effective production routes. It is known that transition metal oxide-based anodes demonstrate a high irreversible capacity at the first cycle and low Coulombic efficiency [21–23].

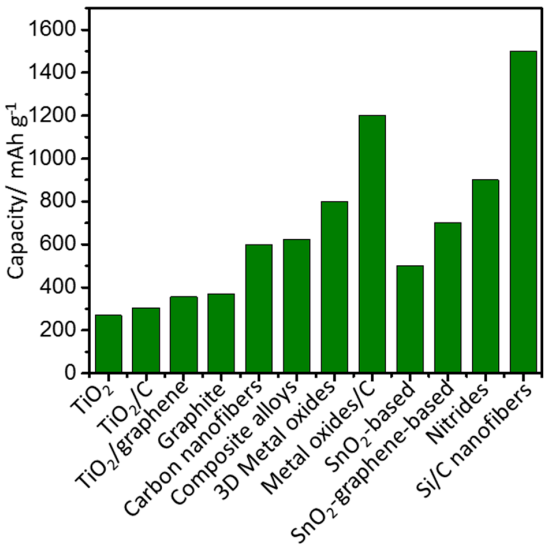

Figure 1. Comparison of the reversible capacity of some anode materials for lithium ion batteries.

TiO_2-based materials are being pioneered as negative electrodes capable to overcome the disadvantages of graphite due to their enormous structural stability. This property is related to their negligible or little volume change during cycling (≈4%), stable capacity retention, and fast kinetics for lithium ion insertion/removal [24,25]. Furthermore, the formation of lithium dendrites is effectively suppressed due to the higher delithiation potential (1.7 V vs. Li/Li^+) making TiO_2 a safe anode material appropriate for various applications. These characteristics are strongly desired to manufacture LIBs in large quantities suitable for mobile and stationary storage applications. Nevertheless, the poor electrical conductivity, low ionic diffusivity, and low theoretical capacity of TiO_2 (335 mAh g^{-1}) are the main obstacles hindering the production of high-performance LIBs with titania anodes [24,26]. The reported reversible capacity of bulk TiO_2 is only 180 mAh g^{-1}, i.e., half of its theoretical capacity [27,28]. Further Li ion storage into the TiO_2 framework is restrained because of the strong repulsive forces among the Li ions. Lithium ion insertion/removal in TiO_2 materials is a diffusion controlled process, which depends on the diffusion coefficient and the diffusion length of TiO_2 [27,29–31]. The diffusion coefficient is determined by the nature of the materials and the diffusion length depends on the particle size of TiO_2. Therefore, many excellent reviews have been reported on the synthesis of various TiO_2 nanostructure

anodes such as nanoparticles, nanotubes, and nanowires of pure titania or as composites with other materials for the application of lithium ion batteries [20,27,32,33]. In the following sections, basics concepts of lithium ion battery systems, various TiO_2 nanostructures, and detailed information about anodically fabricated TiO_2-based negative electrodes are discussed, as they represent the main focus of this review.

2. Lithium Ion Battery System

Generally, a lithium ion battery is a device able to convert chemical energy to electric energy, and vice versa, through electrochemical reactions (oxidation/reduction) between the active materials (anode/cathode) that have a potential difference in the presence of an electrolyte. As described in Figure 2, a LIB is composed of three main components: two electrodes with different electrical potential, and a separator, which electrically isolates the electrodes from each other and allows the Li ions to migrate between the electrodes. The electrolyte is mainly the liquid negotiating medium between the electrodes allowing the migration of Li ions while the separator is completely soaked with the liquid to also avoid being a Li ion barrier.

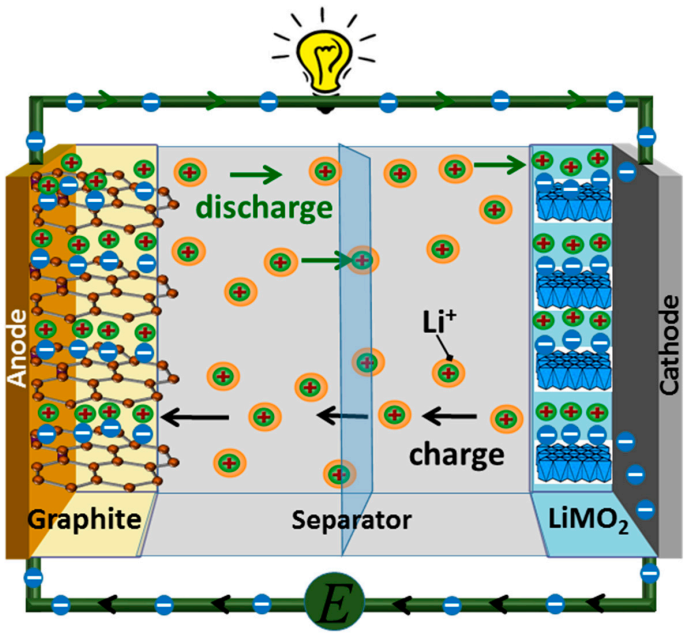

Figure 2. Schematic of the operation principles for rechargeable lithium ion batteries.

In commercial cells, the negative electrode (anode) is composed of intercalation compounds that can host lithium ions i.e., carbonaceous materials. The positive electrode (cathode) consists of other intercalation materials that have more positive redox potential such as lithium transition metal oxides, e.g., $LiMO_2$, M = Co, Ni, Mn, or lithium transition metal phosphates e.g., $LiFePO_4$ or $LiFePO_4$/C composites [34–38]. The electrolyte is commonly composed of a solution, containing a lithium salt (i.e., $LiPF_6$) and mixed with liquid alkyl carbonates [34]. The electrochemical reactions of the electrodes undergo a process, in which Li ions are transported between the cathode and the anode (see Figure 2), and accordingly these processes are called "rocking-chair" reactions [39]. During discharging, Li ions de-intercalate from the anode material and the ions are transported through the electrolyte to intercalate into the cathode, which also acts as electron acceptor [40]. Accordingly, the electrons are shuttled through the external circuit providing the current flow. This process is thermodynamically favorable due to the reduction of the cathode materials in which they spontaneously convert from unfavorable high to an energetically more favorable lower valance. On charging, Li ions de-intercalate in reverse from the cathode to re-intercalate into the negative electrode (anode), which acts as electron donor [41].

This oxidation requires an external trigger, which allows a reaction of the anode material to its previous state.

Table 1 shows the superiority of LIBs over other commercial battery systems explained by specific capacity (Wh kg^{-1}) and energy density (Wh L^{-1}) [42]. Although Li-based batteries have received extensive attention at both fundamental and applied research levels, further improvement in their electrochemical performance is still required. The latter is hindered by some restrictions in the electrode materials and the electrolyte composition. The electrode materials represent the most important part for development as they mainly determine the efficiency of batteries. To construct high performance LIBs, the electrode materials should meet the following requirements: (1) High surface area and large pore size, as they are important to provide a large exposed surface and more channels for lithium ion migration. This results in short paths and faster diffusion rates for lithium ions that play a crucial role to improve the rate capability. (2) Low volume expansion/shrinkage during lithium insertion/extraction to avoid the cracking and miscontacting between the current collector and the electrode materials to increase the cycling stability. (3) High ionic and electrical conductivity which is required to achieve fast charging and discharging as well as facilitating Li ion insertion. (4) High abundance of the composing materials. (5) Low production costs. (6) Environmentally friendly or easily recyclable.

Table 1. Specific energy and energy densities of commercial rechargeable batteries. Reprint with permission [43]; 2017, American Chemical Society.

Rechargeable Battery	Specific Energy, Wh kg^{-1}	Energy Density, Wh L^{-1}
Pb–acid	30	80
Ni–Cd	40	90
Ni–MH	55	165
Ni–Zn	70	145
Ag–Zn	75	200
Li ion	265	690

3. TiO_2 Anodes

TiO_2 has eight known polymorphs: rutile, anatase, brookite, TiO_2-B, TiO_2-R, TiO_2-H, TiO_2-II, TiO_2-III [44]. Among them rutile, anatase and TiO_2-B have been intensively reported as anode materials for lithium ion batteries over the last decades. Rutile is the most thermodynamically stable phase while anatase and TiO_2-B are characterized by a metastable nature [45]. However, previous studies showed that nanosized anatase (below 20 nm) is the thermodynamically most stable [46]. At temperatures higher than 600 °C, anatase undergoes a phase transformation to rutile [47]. The electrochemical lithiation/delithiation of TiO_2 polymorphs are described by Equation (1) [29].

$$x\ Li^+ + TiO_2 + x\ e^- \leftrightarrow Li_xTiO_2\ (0 \leq x\ \text{(mole fraction)} \leq 1) \quad (1)$$

The delithiation reactions strongly depend on the crystallinity, particle size, morphology, surface area, and the involved polymorph. For instance, negligible amounts of Li ions (0.1 Li per Ti atom) are inserted into the rutile structure at room temperature owing to Li ion diffusion into rutile, which is thermodynamically favorable only along the *c*-axis channels instead of the *ab*-planes [30,48]. The crystal structures of rutile, anatase and TiO_2-B are shown in Figure 3. Rutile crystallizes in a tetragonal symmetry with the space group $P4_2/mnm$ with TiO_6 octahedra sharing edges along the *c*-direction while the corners are located along the *ab*-planes [49]. A slight orthorhombic distortion is found for the TiO_6 octahedra [50]. During intercalation, Li ions migrate into the tetrahedral sites neighbored to the *ab*-planes. This property explains the difficulty of the Li ions to reach the TiO_6 octahedral sites [30]. Therefore, the diffusion coefficient through the *c*-direction is 10^{-6} cm^2 s^{-1} which is much larger than that of the *ab*-planes with 10^{-14} cm^2 s^{-1} [30,48,51]. With time, Li ion insertion into the rutile bulk is inhibited and is finally disabled due to repulsion forces between the lithium ions and only low capacities are obtained [30].

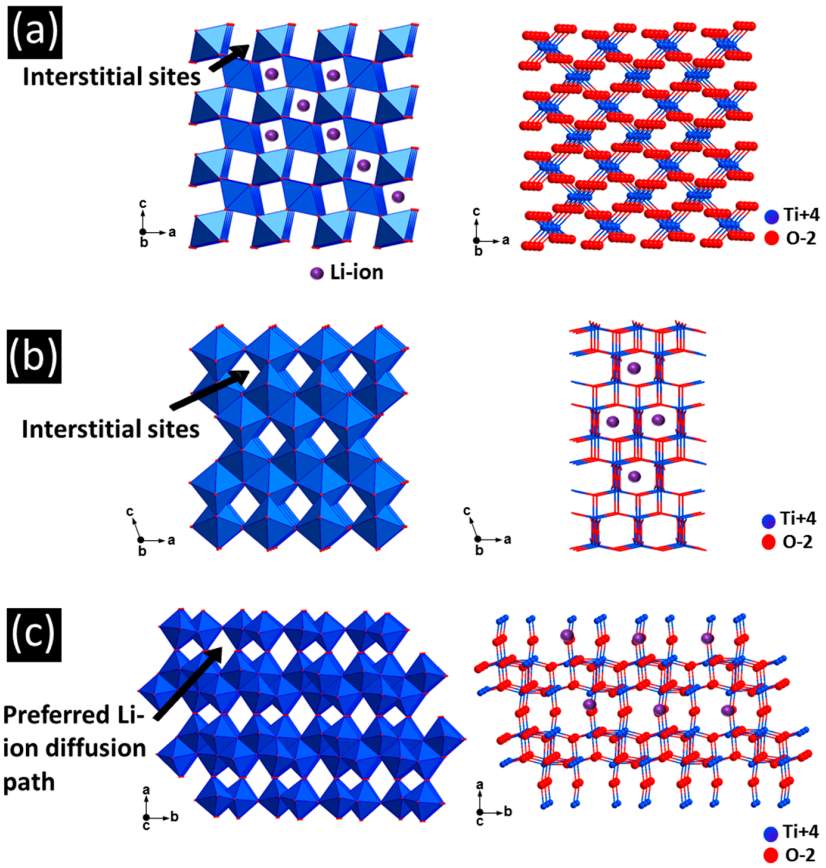

Figure 3. Structure of (**a**) rutile, (**b**) anatase and (**c**) TiO_2-B. The arrows point to the interstitial sites that can host lithium ions.

TiO_2-B has a monoclinic structure with *C*2*m* symmetry, which contains corrugated sheets of edge- and corner sharing TiO_6 polygons [52]. A distorted squared-based pyramid replaces the octahedra due to some long Ti-O bonds (2.20–2.25 Å), which are larger in both anatase (1.937–1.966 Å) and rutile (1.946–1.983 Å) [53]. The open structure of TiO_2-B provides one-dimensional infinite channels, which can accommodate the volume changes during lithium ion insertion without lattice deformation [54]. Pseudocapacitive behavior was also reported for TiO_2-B, which results in a faster diffusion rate during charging/discharging [55].

Anatase has a tetragonal structure with the space group $I4_1/amd$, in which distorted edge-sharing TiO_6 octahedra are stacked in one-dimensional zigzag chains [24,56]. The empty TiO_6 zigzag channels represent diffusion paths for Li ion intercalation. Usually, a phase transition in the tetragonal anatase phase takes place due to the strong Li-Li repulsive forces resulting in an orthorhombic distortion [50,56]. Owing to the Li^+ insertion into the structure, anatase exceeds $Li_{0.05}TiO_2$. The changes of unit cell induced by Li ion intercalaction usually result in decreasing the *c*-axis and increasing the *b*-axis but the total volume changes for the Li ion insertion is less than 4% due to the low total Li content [24].

4. TiO_2 Nanostructures for LIBs

4.1. TiO_2 Nanoparticles

TiO_2 nanoparticles have been approved as effective anode materials in LIBs. The particle size of TiO_2 represents the key factor, which defines reversible capacity and rate performance. When the particle size decreases to nanometer ranges, the surface area increases in consequence and the lithium ion diffusion path is shortened resulting in an improved Li ion insertion capacity. Wagemaker et al. [57] reported on a comparative study among TiO_2 nanoparticles with different crystal particle sizes

(7–40 nm) to explore the impact of particle sizes on the insertion reactions. They found a dramatic increase of Li capacity and Li ion solubility with decreasing sizes of the TiO_2 nanoparticles. Moreover, the small particle sizes improve the rate capability of the electrodes. Figure 4a schematically explains how anatase microparticles can accommodate only up to half a mole of Li ions while the nanosized particles can deliver up to one mole of Li ions per mole TiO_2 [57].

Very fine anatase particles with an average size of 6 nm and a specific surface area of 258 m^2 g^{-1} showed an even higher specific capacity in comparison with particles of 15 and 30 nm in diameter and specific areas of 83 and 57 m^2 g^{-1}, respectively, as shown in Figure 4b. Besides that, the rate capability was also increased by decreasing the particle size [58]. Several studies reported that the kinetics of Li ion insertion significantly depend on the crystallite size [57,59–62]. The phase diagram of various compositions of lithiated TiO_2 versus particle size explains that the particles with 7 nm size or smaller are fully transformed into Li_1TiO_2 reaching the maximum theoretical capacity [57]. Generally, in nanomaterials, the insertion reaction strongly depends on the energetics of the phase boundaries. During the lithiation process of small anatase nanoparticles, only one phase is present in a single particle i.e., anatase or Li-titanate without phase boundaries in this particle [57]. The absence of phase boundaries in small particles is the main reason for the enhancement of Li ion solubility and the solid solution behavior in the single-phase particles. Additionally, the surface strain that occurs between the different intercalated phases is thermodynamically suppressed in small particles. Similar behavior was also experimentally noticed for rutile supported with simulation studies [63]. Jamnik and Maier [64] reported that in small particles (<100 nm), the outer particle surface tension affects the thermodynamics of the Li ion insertion. Size-dependent performance of rutile nanoparticles was investigated by Jiang et al. [65]. The highest initial capacity of about 378 mAh g^{-1} is demonstrated for rutile with a particle size of 15 nm (Figure 4c) at 0.05 A/g. A capacity of 207 mAh g^{-1} was retained after 20 discharging cycles.

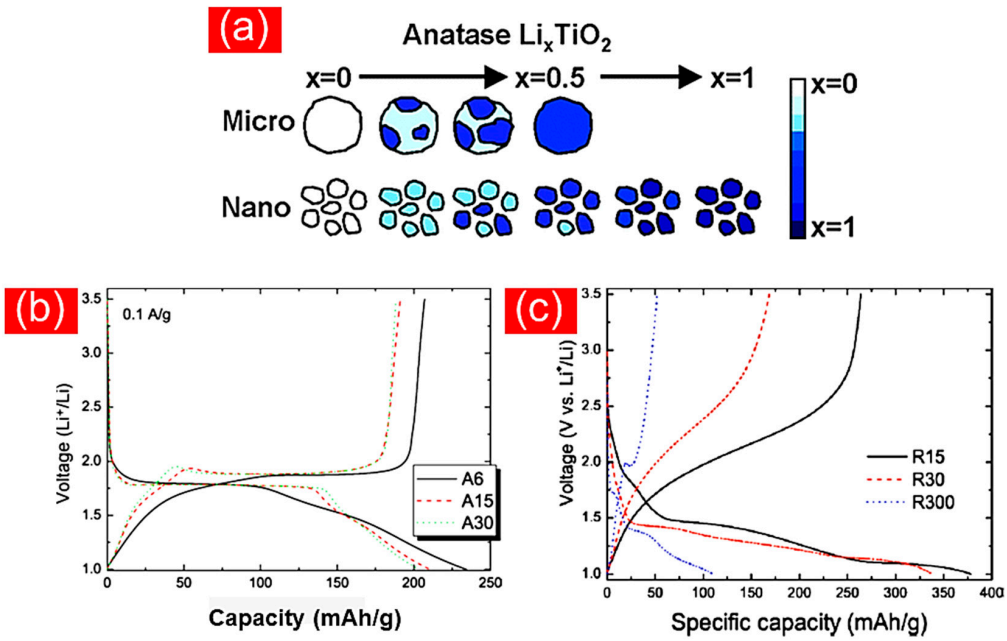

Figure 4. (**a**) Schematic of the impact of particle sizes on the insertion capacity of anatase reprinted with permission from ref. [57]; (**b**) Voltage profile of anatase nanoparticles with 6 (A6), 15 (A15), and 30 (A30) nm in diameter, adapted with permission from ref. [58]; (**c**) The initial capacity profiles of rutile nanoparticles with 15 (R15), 30 (R30), and 300 (R300) nm in diameter, adapted with permission from ref. [65].

Theoretical modeling studies were performed by Sushko et al. [66] to investigate the relation between particle size and ionic conductivity of TiO_2. These studies demonstrated that the ionic conductivity is remarkably improved if the particle size of TiO_2 is below 20 nm due to the higher charge transport of Li ions and electron accumulation on the nanoparticle boundaries. In contrast, when the nanoparticles are larger than 20 nm, charge separation is dominant, hence lower ionic conductivity is obtained [66]. Similar behavior was also found for anatase microparticles [57].

To prepare nanoparticles, the TiO_2 morphology in terms of particle size and surface area was controlled by different synthesis techniques such as sol-gel and solvothermal methods. For instance, Kubiak et al. [67] used sol-gel and mini-emulsion processes to produce mesoporous TiO_2 with different particle sizes (9–12 nm) and pore diameters (7–15 nm). The electrochemical tests showed the lithium insertion capacity is dramatically improved by high surface area and small particle sizes [67]. The authors also found that there is a relation between particle size and the pseudocapacitive effect, where double layer capacity and pseudocapacitity are also increased by reducing the particle size. Nanocrystalline anatase with an average particle size of 5 nm displayed an enhanced Li ion storage capacity compared to 10 nm sized. In addition, faster charging and discharging rates were observed for these nanoparticles owing to the Faradaic reactions, which occur at the electrode surface and control the whole insertion reactions. Similar improvement in electrochemical performance of anatase nanoparticles with average sizes of 8 nm, prepared by the hydrolysis of an organotitanium precursor solution through a sol-gel process with subsequent spray-drying or a hydrothermal treatment was reported by Wilhelm et al. [68]. The prepared nanoparticles can deliver up to 140 mAh g^{-1} at 0.1 C. Anatase nanoparticles prepared by a tenside-assisted hydrolysis with a solvothermal after treatment procedure were tested as anodes and showed a reversible capacity of 196 mAh g^{-1} sustained over 100 cycles at a current rate of 0.2 C [69].

However, formation of TiO_2 particles in the nanoscale is not always useful to improve its Li ion storage, as there is an optimal size range which can positively affect their performance and other sizes do not. For instance, well-dispersed anatase nanoparticles fabricated by a sol-gel method exhibited a considerable enhancement in their Li ion insertion ability when the particle size ranged between 8 and 25 nm [70].

Great interest was paid to further improve the lithium storage performance of zero dimensional TiO_2 by coating the TiO_2 surface with carbon to overcome the poor lithium ion diffusivity and low electrical conductivity. In typical traditional synthesis methods, incorporation of carbon into TiO_2 is conducted by hydrothermal heating of metal salts in the presence of carbon sources such as glucose. However, controlling the carbon content as well as obtaining a homogeneous carbon distribution over the TiO_2 surface is hardly achieved. Lui et al. [71] reported on the hydrothermal carbon-coating treatment to fabricate a sandwich-like structure of a TiO_2@C hollow sphere composite. As a result of combining carbon and TiO_2, the TiO_2@C hollow spheres showed enhanced reversible capacity (240 mAh g^{-1}) with good capacity retention and high rate capability compared to the lower capacity (120 mAh g^{-1}) of uncoated TiO_2 commercial nanoparticles (Degussa P25). Incorporation of carbon into porous TiO_2 nanoshells was studied by Wang et al. [72] who succeeded in controlling the carbon content in TiO_2@C composites to realize a highly reversible lithium ion storage (Figure 5a). The preparation procedure includes two steps where in the first one TiO_2 hollow spheres were coated with a resorcinol-formaldehyde layer via a sol-gel method. The second step involves a thermal treatment to carbonize the polymer and to form a crystalline TiO_2 shell. The TiO_2@C electrode showed a capacity of ~425 mAh g^{-1} at a current rate of 0.1 C. The specific capacity of this electrode decreased to ~150 mAh g^{-1} when the current rate was increased to 10 C (Figure 5b). In addition, such a composite demonstrated a reversible capacity of ~190 mAh g^{-1}, which is slightly decreased to 170 mAh g^{-1} after more than 300 charging/discharging cycles at 2 C (Figure 5c). The ability to precisely control the carbon content of theTiO_2@C composites makes this preparation route highly attractive compared to traditional hydrothermal preparations.

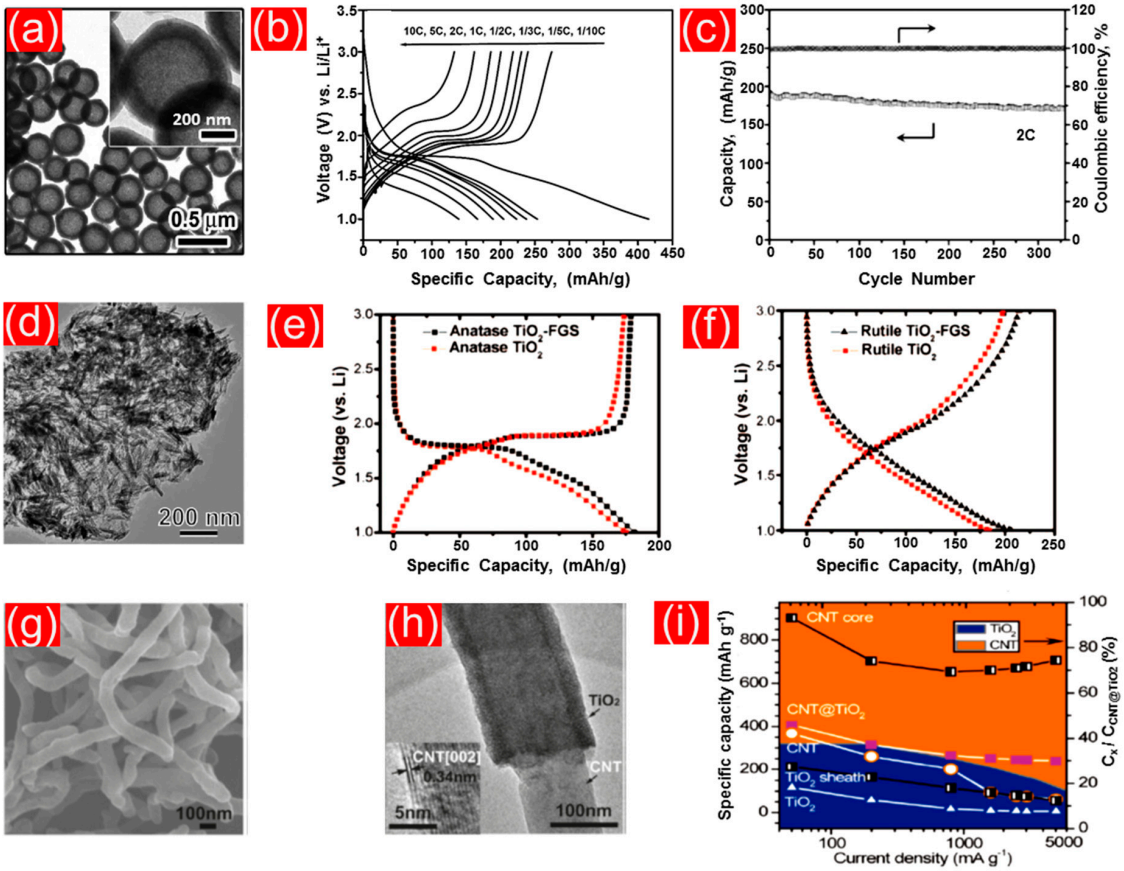

Figure 5. (**a**) Scanning electron microscopy (SEM) image of TiO_2/C shells, (**b**) first discharging/charging voltage profiles at different current densities, and (**c**) cycling performance, adapted with permission from ref. [72]. (**d**) SEM image of TiO_2-functionalized graphene sheet hybrids and their voltage profiles for (**e**) anatase and (**f**) rutile phases, adapted with permission from ref. [73]. (**g**) SEM and (**h**) transmission electron microscopy (TEM) micrographs of TiO_2-coated carbon nanotubes (CNTs) and (**i**) their cycling performance, adapted with permission from ref. [74].

Graphene is a promising candidate of the carbon family for incorporation into TiO_2 as it is considered to show excellent electron transport. Coating of TiO_2 nanoparticles with a graphene layer provides pathways for electron transport resulting in a higher electrical conductivity, which overcomes the internal resistance of TiO_2. Furthermore, these conductive boundaries serve as protective layers to prevent the direct contact between the TiO_2 and the electrolyte followed by an enhanced stability of the active materials and low parasitic electrolyte consumption. Various studies report on the fabrication of TiO_2-graphene hybrid nanostructure for improved Li-ion insertion. Wang et al. [73] used an in-situ technique to fabricate self-assembled nanocrystalline TiO_2 with graphene utilizing anionic sulfate surfactants to stabilize graphene in aqueous solutions (Figure 5d). The obtained hybrid nanostructure showed a doubling of the Li ion insertion capacity of the pure TiO_2 as a result of an increased electrical conductivity induced by graphene (Figure 5e,f). In another study [75], a TiO_2 nanoparticles@graphene composite was prepared in-situ by the hydrolysis of $TiCl_4$ in the presence of graphene oxide nanosheets subsequently reduced by hydrazine hydrate. The obtained TiO_2-graphene composites were tested for Li ion intercalation as anodes demonstrating a reversible capacity of 60 mAh g^{-1} at a high current rate of 5 A g^{-1} with negligible fade over 400 cycles. The unique conductivity of graphene sheets combined with well-dispersed TiO_2 nanoparticles led to a superior electrochemical performance in Li ion storage.

Owing to their high conductivity, stability, and the ease of manufacturing, carbon nanotubes (CNTs) were used as a further excellent candidate to synthesize highly valuable TiO_2 composite anodes. Core-shell CNTs/TiO_2 (Figure 5g,h) were prepared by hydrolysis of tetrabutyl titanate and showed a

specific capacity of ~240 mAh g^{-1} at a current density of 5 A g^{-1} exhibiting a threefold increase in capacity compared to pure TiO_2 (62 mAh g^{-1}) at the same current density (Figure 5i). The enhancement in capacity was attributed to the better electron supply due to the CNTs enabling the TiO_2 shells to store higher lithium ion concentrations [74].

Excursus: Nanoparticulate TiO_2 Contributions in Redox-Flow Lithium Ion Batteries

The redox-flow battery (RFB) is one of the most promising energy storage systems that provides high capacity and energy density suitable for numerous application e.g., in the automotive sector but is also heavily discussed for large-scale stationary power storage units for renewable power production and grid stability. A typical flow battery is composed of three components, (i) an electrochemical cell-power output unit in which, two adjacent electrochemical half cells, containing porous electrodes are separated by a semipermeable membrane, (ii) two energy storage tanks (anolyte and catholyte) each filled with redox-active species are dissolved in a solvent serving as electrolyte, (iii) a pumping unit which circulates the anolyte and catholyte between the power output cells and the energy storage tanks [76–79]. The operation principle is based on oxidation and reduction reactions between the electroactive transition metal ion species at the surface of a porous electrode in the electrochemical cells. The two electrolyte solutions, which represent the active electrode materials, are pumped into a membrane-divided stack allowing for ion migration of the conducting salt and not the redox-active species and the electron transfer [76–78]. The vanadium redox-flow battery is one of the famous flow battery examples established in the market for large-scale storage [80]. One of the main obstacles hindering the breakthrough of redox-flow batteries in the market is the poor solubility of electroactive species and the dead weight of non-redox-active materials in the electrolyte which limits the energy density of the battery [76,81,82]. A promising approach to increase the energy density of flow batteries was explored by integrating solid lithium intercalation compounds mixed with conductive materials into the flow solutions containing lithium ions [77,79–82]. This approach, known as redox-flow lithium-ion battery (RFLB), bundles together the advantages of the high energy density of lithium ion battery and the flexibility of the redox-flow battery. In such a battery system, the energy is stored in the Li-intercalation materials, as in conventional batteries, which are statically present in the energy storage tanks. TiO_2 has been investigated as anode materials in RFLB. Pan et al. [83] reported the reversible Li-storage of anatase by chemically using two redox mediators, bis(pentamethylcyclopentadienyl)cobalt [$Co(Cp^*)_2$] and cobaltocene [$Co(Cp)_2$]. The Li ions are intercalated into TiO_2 suspended in the electrolyte without attaching TiO_2 onto the electrodes of the flow channel. Anatase delivered a reversible capacity of 0.33 Li ions per TiO_2. Further confirmation of the achieved capacity was obtained by theoretical calculations using density functional theory (DFT). Jia et al. [84] used a full cell configuration of RFLB, in which $LiFePO_4$ and TiO_2 were utilized as the cathodic and anodic materials, respectively. The RFLB exhibited good cycling performance demonstrating an energy density of ~500 Wh L^{-1}. The energy storage ability of RFLB are negatively affected by the formation of a solid electrolyte interface on the electrode surface due to the reduction of the alkyl carbonate of the electrolyte at a potential less than 0.8 V vs. Li/Li^+ resulting in a slow charge transfer, especially when graphite is used as solid anodic material. Using active anode materials with operating voltage higher than the decomposition potential of the electrolyte, such as TiO_2 and $Li_4Ti_5O_{12}$, the formation of the solid electrolyte interface is effectively suppressed and hence, allows for better ionic transport and improved intercalation characteristics [80].

4.2. TiO_2 Nanorods, Nanoneedles, Nanowires, and Nanofibers

The main drawback of TiO_2 nanoparticles as anodes in LIBs is the missing contact between the particle boundaries, which results in poor electronic and ionic conductivity [65,68]. Additionally, the random motion of the electrons through the particles, as there are no defined pathways for the electron transport, hinders the electron separation at the current collectors [70,85]. Furthermore, the nanoparticles with high surface area possess higher surface energies compared to bulk materials.

These particles can aggregate during the synthesis process or even during an electrochemical intercalation and thus the surface area decreases accordingly [85]. Indeed, the formed aggregates restrain the electrolyte in reaching a particle surface causing a severe capacity drop.

Fabrication of TiO_2 with particular one-dimensional morphologies such as nanorods, nanoneedles, and nanowires could significantly overcome the nanoparticles' drawbacks and improve their lithium ion insertion ability. Experimental work showed that the porous nature of the nanowires allows a good contact between electrolyte and electrode material and accommodates the strain resulting from changing the crystal dimensions after the electrochemical insertion reaction. As an example flower-like rutile nanorods (Figure 6a) were synthesized by hydrolysis of a $TiCl_4$/ethanol solution at 50 °C [86]. The obtained nanorods showed a considerably higher reversible capacity and cycling stability than spherical rutile nanoparticles (Figure 6b). The significant improvement in battery performance was attributed to the rod geometry of rutile oriented along the *c*-direction of the unit cell, which is thermodynamically favorable for lithium ion insertion [86]. Fabrication of anatase nanotubes can be performed easily via rutile powders which have been hydrothermally treated at 500 °C and 700 °C in alkaline media (10 M NaOH) (Figure 6c). Reproducible discharging capacity (~175 mAh g^{-1}) was also noticed for anatase nanotubes after 10 cycles at a 0.1 C rate (Figure 6d) [87]. A similar synthesis route was reported by Kim et al. [88]. They further treated the obtained nanotubes/nanorods at a temperature between 300 °C and 400 °C to transform the present nanotubes into nanorods. Bao et al. [89] succeeded in hydrothermally producing porous anatase nanorods at a lower temperature (200 °C) in an alkaline medium using a NaOH/KOH mixture. The resulting nanorods showed a high initial discharging capacity of 212 mAh g^{-1} at a current density of 60 mA g^{-1}, which was retained for 30 discharging/charging cycles. Gao et al. [90] developed a method to prepare anatase nanorods. For this, $TiCl_4$ undergoes a hydrolysis with caustic soda and the obtained hydrolysate is hydrothermally treated at 110 °C. The material exhibited a lithium insertion capacity of 206 mAh g^{-1} with good reversibility at a current density of 50 mA g^{-1}. Rutile nanoneedles with about 25 nm in diameter and 100 nm in length were prepared from titanium isopropoxide by a reverse microemulsion mediated sol-gel method (Figure 6e). The nanoneedle electrode was capable of achieving an initial specific capacity of 305 mAh g^{-1} (Figure 6f) [91]. Wang et al. [92] reported on the fabrication of anatase nanowires with a minor TiO_2-B phase content via the hydrothermal treatment of commercial P25 powders (Degussa) followed by an annealing step at 400 °C (Figure 6g). These nanowires demonstrated a high specific capacity of 280 mAh g^{-1} at a current density of 140 mA g^{-1} upon 40 cycles with a Coulombic efficiency of 89% (Figure 6h). Wu et al. [93] developed a room temperature hydrothermal method without using a Teflon-lined autoclave to prepare anatase nanowires from $Ti(OC_4H_9)_4$. This material was characterized with a reversible capacity of 216 mAh g^{-1} at a current density of 20 mA g^{-1}. Anatase particles were converted into TiO_2-B nanowires with diameters ranging from 20 to 40 nm by a hydrothermal method in the presence of an aqueous solution of NaOH [94].

A binder-free electrode composed of TiO_2 nanofibers was prepared by an electrospinning technique followed by a calcination step at 400 °C in air [95]. The TiO_2 nanofibers showed a specific capacity of 175 mAh g^{-1} at a current rate of 0.3 C with a Coulombic efficiency between 96% and 100% over 50 cycles.

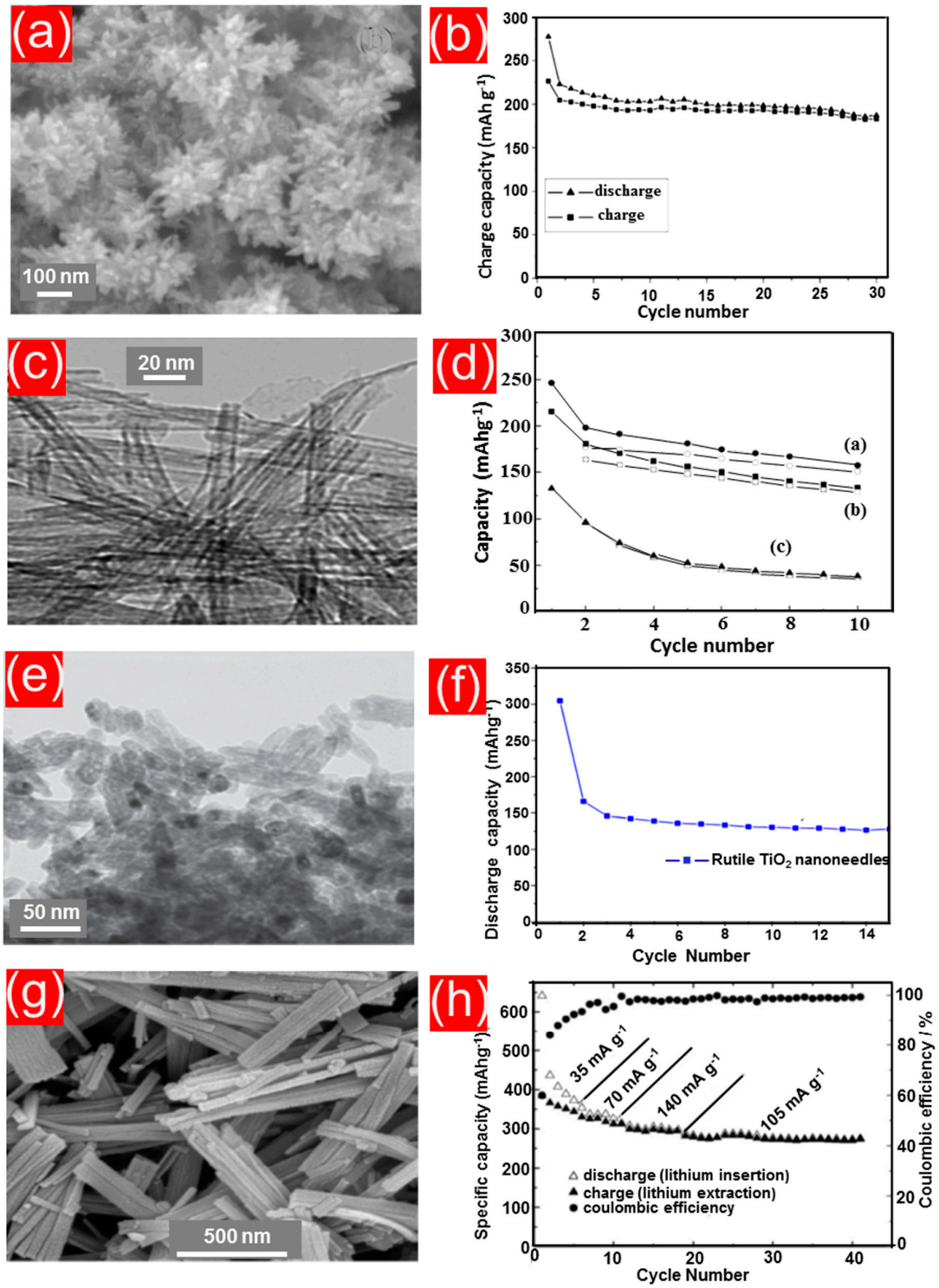

Figure 6. (**a**) SEM image of the flower-like rutile nanorods and (**b**) their galvanostatic cycling at 0.1 C adapted with permission from ref. [86]. (**c**) TEM image of TiO_2 nanotubes synthesized by treating of rutile with NaOH at 125 °C and (**d**) their performance denoted in image with symbol (**a**) adapted with permission from ref. [87]. (**e**) TEM image of as-prepared rutile nanoneedles, (**f**) their discharge cycling and voltage profiles appear in the inset adapted with permission from ref. [91]. (**g**) SEM image of the as-prepared TiO_2 nanowires, their discharging capacity and (**h**) Coulombic efficiency at different current densities adapted with permission from ref. [92].

The electrochemical performance of 1D TiO_2 nanoarchitectures can be further improved by coating or doping with carbonaceous materials that improve both the electrical and ionic conductivities. Goriparti et al. [96] synthesized carbon-doped TiO_2 nanowires by a hydrothermal method and employed them as anodes in LIBs. The as-prepared C-doped TiO_2 nanowires offered enhanced reversible capacity of 306 mAh g^{-1} at a current rate of 0.1 C with long term cycling (1000 charging/discharging cycles) compared to the undoped TiO_2 nanowires. Controlled hydrolysis was developed by Shen et al. [97] to fabricate a 3D hybrid nanocomposite of TiO_2-graphene-CNTs. This study showed that combining conductive graphene sheets and CNTs results in an excellent electron transport and supports Li ion intercalation into TiO_2 nanoparticles. A specific capacity of ≈120 mAh g^{-1} was obtained at a high current rate (10 C) maintained for 100 cycles. The hybrid electrode also exhibited a significantly high rate capability when tested at various current rates from 0.5 to 30 C.

As already explained, high conductivity and good electron transport, especially at high temperature, positions graphene as a good additive to form composites with TiO_2 in order to reduce the internal resistance and decrease the irreversible heat which is produced from charging and discharging processes. TiO_2 nanotube@graphene composites were explored by Wang et al. [98] prepared by a single-step hydrothermal synthesis. The composites presented a high storage capacity of 357 mAh g^{-1} at 10 mA g^{-1} when used as anodes in LIBs. The tubular structure of TiO_2 and the good electronic properties of graphene are the main reasons behind the excellent performance of such a composite. In addition, TiO_2 nanorod arrays were grown onto graphene sheets by a modified seed-assisted hydrothermal preparation. A sandwich-like nanocomposite of rutile nanorods/graphene was observed exhibiting largely improved reversible charging/discharging capacities and an enhanced robust rate capability compared to pure TiO_2 nanorods. The observed better performances were mainly attributed to superior conductivity and the unique structure of such a composite that supports excellent insertion reactions [99]. Zuniga et al. [100] produced multichannel hollow nanofibers of a TiO_2/C composite by a force spinning process, in which polyvinylpyrrolidone (PVP) and titanium (IV) butoxide were used as precursors. The as-formed precursor-based nanofibers were thermally treated at 280 °C in air and subsequently with another carbonizing step at 550 °C in the presence of argon atmosphere to finally obtain TiO_2/C. The binder-free electrode from this nanocomposite demonstrated a specific capacity of ≈229 mAh g^{-1} when cycled at a current density of 100 mA g^{-1} with a Coulombic efficiency of 98% after 100 charging/discharging cycles. The authors ascribed the superior cycling performance of the TiO_2/C hollow nanocomposite to the increased reactive sites due to the high surface area (123 m^2/g) of the one-dimensional hollow nanofiber compared to non-hollow TiO_2/C (61 m^2/g), as well as the reduced diffusion length of the Li^+ ions to achieve a higher Li ion intercalation. Thirugunanama et al. [101] fabricated graphene-wrapped TiO_2 nanofibers by electrospinning. The graphene/TiO_2 nanofibers showed a doubled surface area according to the Brunauer-Emmett-Teller model compared to pure TiO_2 nanofibers before wrapping with graphene (54 m^2 g^{-1}). High reversible capacities of up to 200 mAh g^{-1} were demonstrated at a current rate of 0.1 C. Meanwhile, pure TiO_2 nanofibers delivered only 160 mAh g^{-1} at the same current density. The porous nature of the material coupled with a high surface area provided more favorable Li ion storage sites. The effect of graphene on the electrical and ionic conductivity helped to achieve high rate performance and reversibility. Ding et al. [102] succeeded in growing ultrathin anatase nanosheets on graphene as support by a solvothermal method. A reversible capacity of up to 161 mAh g^{-1} was demonstrated by this composite anode after 120 charging/discharge cycles at a current rate of 1 C. The unique structure of the composite is closely attributed to the high electrochemical performance. Flower-like nanostructures of a TiO_2/graphene composite were prepared by Xin et al. [103] using a hydrolysis method. The TiO_2/graphene composite demonstrated a capacity of about 230 mAh g^{-1} at 0.1 C exhibiting high rate capability and cycling stability up to a current rate of 50 C in a half cell experiment. TiO_2 nanoparticles with porous texture along with highly conductive graphene enabled fast electron transfer and better Li ion diffusion resulting in outstanding reversibility with average capacity fading of 0.03% per cycle. However, in another study, Choi et al. [104] prepared TiO_2/graphene nanocomposites by self-assembling and

tested them in a full cell configuration versus $LiFePO_4$. The full cell showed ≈125 mAh g^{-1} specific capacity with negligible fade even after 700 charging/discharging cycles when tested at a current rate of 1 C.

4.3. Porous TiO_2 Nanostructures

Application of porous TiO_2 nanostructures is another promising approach to decrease the diffusion paths of Li ions in the electrode material and, thus, develop their insertion performance. The specific nature of porous nanostructures and the high surface area allow for good wettability and better permeability of the electrolyte, facilitating excellent charge transfer across the electrode material at the electrode/electrolyte interface. Particular attention has been paid to synthesize nanoporous TiO_2 with different morphologies including 0D, 1D, 2D, and 3D structures. To generally show the positive effect of porosity in 0D nanostructures, porous TiO_2 nanospheres were fabricated by a simple sol-gel method followed by thermal annealing. The electrochemical measurements indicate that the obtained material with such a porous structure was able to deliver higher reversible capacities than dense TiO_2 nanospheres without porosity [105]. The fabrication of such porous structures is commonly performed by template-free and template-assisted methods [54]. In the template-free approach, a hydrothermal process is used to obtain core-shell structured mesoporous TiO_2 spheres while in the template-assisted procedure, surfactants are utilized. The main advantages of this preparation route are the ability to fabricate well-ordered and uniform mesopores with high surface area. Zero-dimensional (0D) nanoporous hollow spheres were synthesized using carboxyl functionalized polystyrene TiO_2 spheres as a template (Figure 7a). As anode materials, such hollow spheres showed a reversible capacity of 230 mAh g^{-1} when cycled at a current density of 33.5 mA g^{-1} (Figure 7b). With this measure, additional surface capacities may be generated for such porous structures resulting in good Li ion storage properties [106]. The relation between porosity and lithium storage characteristics was investigated by Saravanna and co-workers [107]. They fabricated various mesoporous TiO_2 nanoparticles (10–20 nm particle size) with different pore sizes (5.7–7 nm) by a soft template method in which titanium isopropoxide was selected as a titanium source with different cationic surfactants of various chain lengths. The specific surface area of the prepared samples increases from 90 to 135 m^2 g^{-1} with increasing pore diameters. The electrochemical results showed a high specific capacity of 268 mAh g^{-1} of the sample with the highest surface area. The improved performance was ascribed to the high surface area which provides much larger voids for increased Li ion accommodation. Wang et al. [108] developed a facile microwave-assisted hydrothermal method to produce porous TiO_2 spheres with a subsequent annealing step at 500 °C. When tested as electrodes in LIBs, they showed a stable Li ion storage capacity of 184 mAh g^{-1} at 1 C.

Indeed, coating 0D mesoporous TiO_2 with carbon, as often utilized, not always results in a high specific capacity. For instance, Zhang et al. [109] reported the synthesis of a C-coated mesoporous TiO_2@graphene sheets composite via a one-step solvothermal synthesis. The sandwich-like structure of this hybrid composite was applied as electrode for LIBs exhibiting an initial capacity of 145 mAh g^{-1} at a current density of 0.2 A g^{-1}. Only a specific capacity of 111 mAh g^{-1} was achieved after 100 cycles.

One-dimensional (1D) structures of TiO_2 with a mesoporous rod-like morphology were reported by Jiang et al. [110] by ultraviolet irradiation of titanium glycolate previous to a heat treatment. A reversible capacity of 161 mAh g^{-1} at a current density of 1 A g^{-1} was demonstrated and retained for 40 cycles. Anatase nanorods were also synthesized by a low temperature colloidal synthesis from a thermal decomposition of titanium precursors containing a coordinating agent such as oleic acid. In this preparation route oleic acid is utilized as a capping agent to prevent the nanoparticle agglomeration during the synthesis process as well as providing a carbonaceous percolating network to cover the porous nanorods. The electrode composite showed a specific capacity of 250 mAh g^{-1} at a rate of 1 C confirming the superiority of such a porous, coated structure [111]. Core-shell nanocomposites from mesoporous Fe_2O_3 nanorods-TiO_2 were synthesized by thermal treatment of FeOOH@TiO_2 [112]. The composite electrode delivered a reversible capacity of 860 mAh g^{-1} at a current density of 1 A g^{-1}

demonstrating a prolonged cycling stability over 1000 charging/discharging cycles. The high capacity obtained by such an electrode was attributed to the unique structure with the mesoporous texture of the composite as well as the synergetic effect originating from the high capacity of the Fe_2O_3 core with a durable TiO_2 shell. In another study, Wang et al. [113] succeeded in fabricating hierarchical TiO_2/Fe_2O_3 fiber-in-tube architectures with a TiO_2 fiber as the core and Fe_2O_3 as the shell by electrospinning. High initial capacities of up to 987 mAh g^{-1} were demonstrated at a current density of 100 mA g^{-1} with 65% capacity retention after 240 cycles.

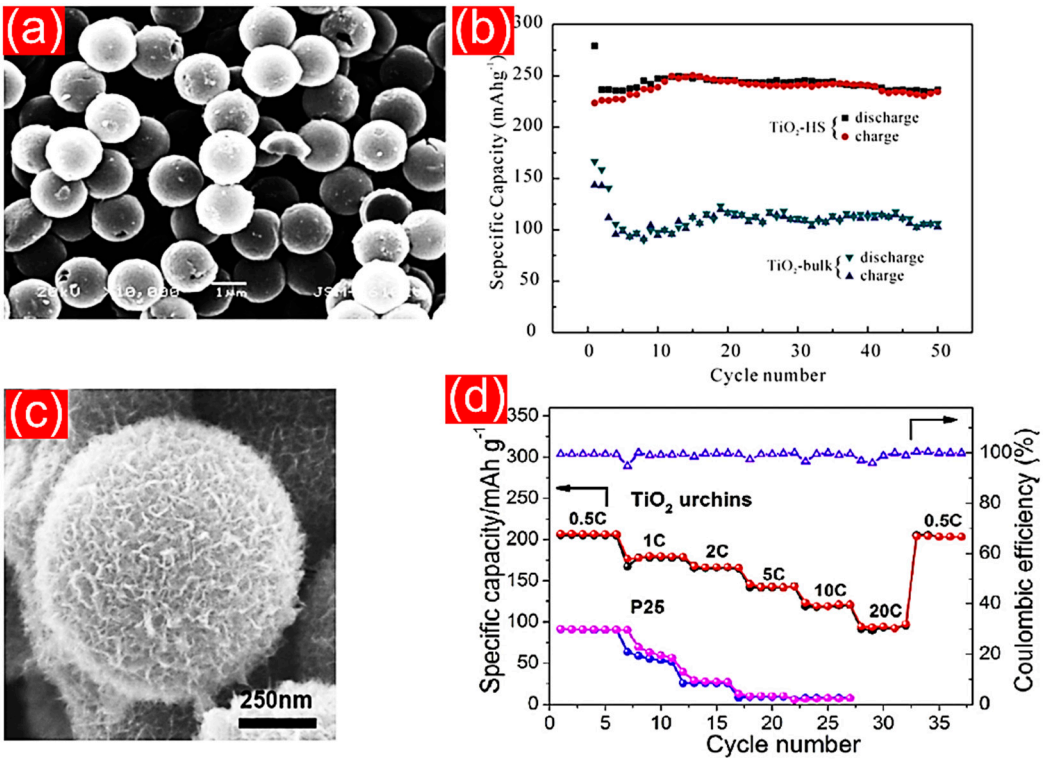

Figure 7. (**a**) SEM micrograph and (**b**) galvanostatic cycling of TiO_2 hollow spheres (HS) in comparison with bulk TiO_2 at 0.1 C adapted with permission from ref. [105]. (**c**) SEM image and (**d**) rate capability of the porous TiO_2 urchins compared to commercial P25 nanoparticles adapted with permission from ref. [114].

Hierarchically ordered porous TiO_2 with 2D structures have received great interest especially as negative electrodes in LIBs. These unique porous nanostructures provide a rapid reactant transport through the larger pore diameters as well as a high surface area which is obtained from the smaller pores acting as active sites for the adsorption/desorption of the reactants. Recently, 2D hierarchically ordered porous anatase with a specific surface area of 486 m^2 g^{-1} was synthesized by chemical etching of amorphous TiO_2 powder using acetic acid [115]. The obtained texture is defined by micropores with a range of 2 to 6 nm and mesopores of 15 to 80 nm. A reversible specific capacity of 191 mAh g^{-1} was demonstrated for this hierarchical structure at a current rate of 1 A g^{-1} and this capacity is retained for 60 cycles [115]. Higher capacity obtained by hierarchical, porous anatase structures with high surface area and uniform pore size distribution compared to nonporous TiO_2 is attributed to Li^+ ion intercalation in the conventional octahedral sites of the bulk material and an additional storage possibility in extra sites at interfaces. Jamnik and Maier [64,116] proposed a storage mechanism which is called 'Job-sharing' to explain how the reversible Li ion storage capacity is achieved at the interfaces of the hierarchical TiO_2 nanostructures with high surface areas. This mechanism explains why lithium ions are stored in the accessible interstitial sites of the electrode, whereas the electrons are stored in another phase, such as the conductive carbon additives or the SEI layer [117]. The synergetic effect of a

lithium ion-accepting and an electron-accepting phase triggers additional storage capacity through the ease of charge separation [117,118]. This interfacial capacity phenomenon is kinetically favored for the nanostructure with high volume fractions of interfacial areas, especially when the electrode is directly cycled at high current rates without starting with a low rate at first [117]. Jin et al. [118] prepared hierarchical nanosheets with a yolk-shell structure arranged as a highly porous microsphere shell and a dense mesoporous core by a solvothermal alcoholysis. The pore diameter of the outer 2D nanosheet shell is about 15 nm and of the inner mesoporous core of about 3 nm. These particular structures offer a stable porous framework that allows for electrolyte diffusion by capillary attraction and also buffer the volume increase along with the lithium ion intercalation/extraction reactions. Prolonged galvanostatic cycling over 700 cycles was performed by such an electrode exhibiting a reversible specific capacity of 225 mAh g^{-1} [118].

Three-dimensional (3D) porous structures were also studied for the application in lithium ion storage. The synthesis of 3D interconnected hierarchical structures composed of porous urchins was reported by Cai et al. [114] (Figure 7c) and was performed hydrothermally from TiO_2 and oleylamine as precursors followed by an ion-exchange and a calcination process. When evaluated as anode material, the 3D structure showed a lithium ion storage capacity of 206 mAh g^{-1} at 0.5 C after 100 cycles (Figure 7d). The formation of 3D hierarchical nanoporous anatase via the hydrolysis of titanium glycolate was reported by Shin et al. [117]. A lithium ion storage capacity of 302 mAh g^{-1} was observed for such microporous anodes with superior cycling stability. The experimental results of this study have proven that 64% of the achieved capacity is attributed to two major storage processes which are bulk insertion and pseudo-capacitive interfacial storage modes. The electrochemical performance of such a material reflects the importance of the high surface area of microporous TiO_2 in generating additional pseudo-capacitance. Recent work demonstrated a simple in-situ preparation of ordered 3D macroporous TiO_2 anodes using a polystyrene templated carbon cloth. The 3D electrodes provided a specific capacity of 174 mAh g^{-1} when cycled at a current density of 2 A g^{-1} [119]. The pore size and the thickness effects on the electrochemical performance of the 3D porous electrodes were prepared by atomic layer deposition and optimized during a systematic study of Ye et al. [120]. The results revealed that decreasing the pore sizes and thickness of the 3D electrode, improved its power performance and the diffusivity of Li ions across the electrode/electrolyte interface.

4.4. TiO_2 Nanotubes Prepared by Electrochemical Anodization

The one dimensional (1D) tubular structure of TiO_2 is of great scientific interest as well as practical significance particularly when the nanotubes are highly ordered and perfectly aligned in close packed arrays. These outstanding characteristics are realized by the potentiostatic anodization of Ti substrates as it is a simple, straightforward, and cost-effective preparation technique (see Figure 8). The majority of the reported preparation methods only result in random networks of TiO_2 nanotubes with uncontrolled dimensions. However, template-assisted atomic layer deposition (ALD) can produce nanotubes with controlled geometries. This extensive preparation is reflected in the high cost of the resulting product and the operating expense, like the apparatus, and thus, limits the use and the benefit [121].

The first anodic oxidation study of pure Ti metal and Ti-6Al-4V alloy substrates resulted in uniform porous films of TiO_2 as reported by Zwilling et al. [122] in 1999. However, a previous report before Zwilling's work explored the anodization of Ti substrates in the presence of fluoride ions which only resulted in a porous structure [123]. In 2001, Grimes and co-workers [124] succeeded in synthesizing well-defined nanotube arrays by the anodic oxidation of Ti substrates in an HF-containing electrolyte. These results aroused a lot of attention and pushed the research towards the optimization of synthesis parameters (i.e., electrolyte configurations, applied voltage, reaction time, pH, agitation, and temperature, etc.), to understand the formation mechanism and to employ these nanotubes in various research-near applications.

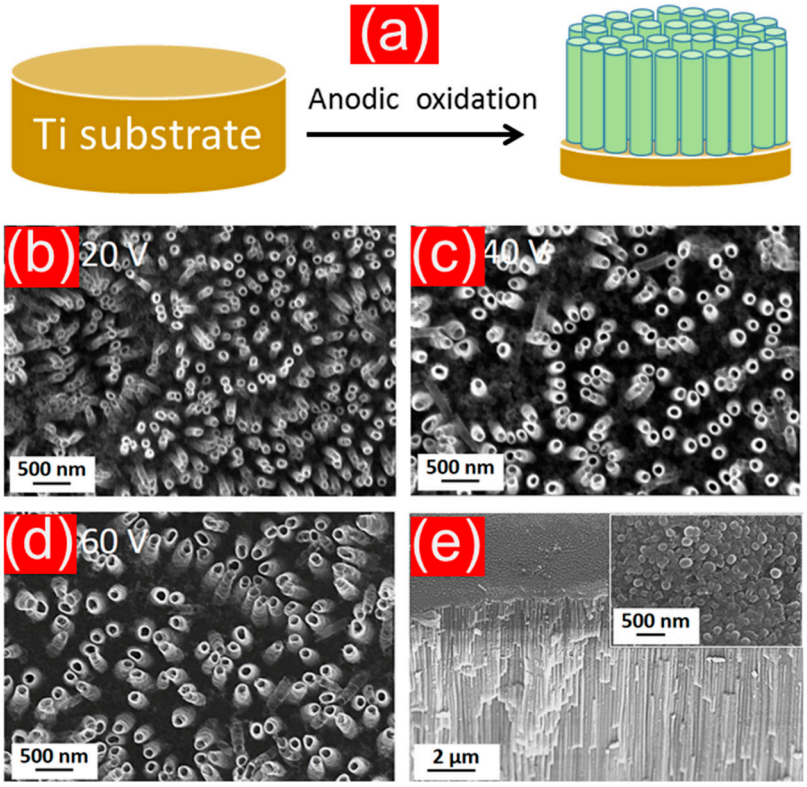

Figure 8. (**a**) Schematic illustration of the formation of TiO_2 nanotubes by the anodization of a Ti substrate. SEM micrograph of anodized Ti substrates in formamide-based electrolyte containing 0.2 M NH_4F at different anodization voltage (**b**) 20 V, (**c**) 40 V, and (**d**) 60 V. (**e**) The cross-sectional view while the inset shows the bottom view of the nanotubes prepared at 60 V reprinted with permission from ref. [125].

Extensive studies proved that the TiO_2 nanotubes obtained by anodic oxidation are self-organized, well-aligned perpendicularly to the substrate, and exhibit uniform tube diameters, and wall thicknesses as well as high surface areas. Furthermore, the nanotube dimensions (i.e., diameter, wall thickness, and tube length) can be precisely controlled by tuning the applied voltage, the employed temperature, and the electrolyte composition especially by the F^- concentration [122–127]. The anodization is normally performed in a two-electrode electrochemical cell with the metal or alloy sheets as the working electrode and platinum foil or graphite as counter electrode in aqueous or organic electrolytes containing F^- ions as shown in the schematic of Figure 9. Aqueous HF solutions were first used as electrolytes to manufacture TiO_2 nanotube arrays with tube lengths below 500 nm [123,128]. Replacing the aqueous solutions with organic electrolytes composed of ethylene glycol as main solvent in addition to a fluorine source such as NH_4F at high pH values enables TiO_2 nanotube formation with lengths reaching up to 1 millimeter [128–130].

The nanotubes fabricated with these electrolytes always exhibited average diameters and wall thicknesses larger than 50 nm and 15 nm, respectively. Using neutral electrolytes such as those containing $(NH_4)_2SO_4$ with NH_4F leads to a reduced dissolution rate of TiO_2 resulting in nanotube arrays with lengths in the micrometer range [131]. These electrolytes are known as establishing mild oxidation conditions for the Ti substrates. Please note that the chemical composition of the electrolyte also plays a central role in the physical properties of the fabricated nanotubes [132,133]. For instance, addition of acetic acid results in the formation of robust tubes. Furthermore, increasing the F^- concentration allows control of the tube wall thickness [131,132].

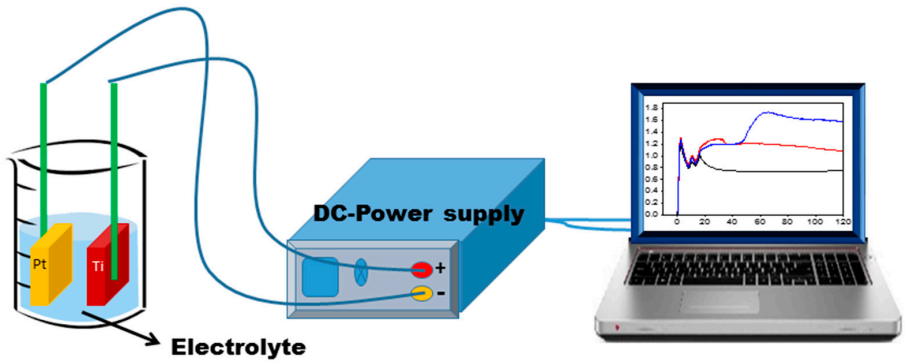

Figure 9. Schematic illustration of anodic oxidation setup.

Excursus: The Mechanism of Nanotube Formation by Anodic oxidation

The formation mechanism of TiO_2 nanotubes is basically similar to the mechanism of formation of porous alumina as roughly described by Equations (2)–(5) [133–135]. At the beginning of an anodization process, the Ti substrate is exposed to the electrolyte and a compact oxide layer of TiO_2 is formed on the substrate surface due to the interaction between Ti metal and H_2O as described in Equation (3a) [107]. In addition, the initially obtained oxide layer is subjected to an electric field-aided dissolution to produce Ti^{4+} cations where, the Ti-O bonds can easily be broken due to the high polarization effect originating from the electric field [136,137].

$$Ti \rightarrow Ti^{4+} + 4e^- \quad (2)$$

$$Ti + 6H_2O \rightarrow TiO_2 + 4H_3O^+ + 4e^- \quad (3a)$$

$$Ti^{4+} + 8H_2O \rightarrow Ti(OH)_4 + 4H_3O^+ \quad (3b)$$

$$Ti(OH)_4 \rightarrow TiO_2 + 2H_2O \quad (4)$$

At the same time, hydrogen evolution occurs at the cathodic side as the complementary reaction according to Equation (5) [138].

$$8H_3O^+ + 8e^- \rightarrow 4H_2 \uparrow + 4H_2O \quad (5)$$

Note that, as soon as the voltage is applied, the electric field induces the anodic dissolution of the Ti surface to form Ti^{4+} ions (Equation (2)) as well as the generation of oxygen anions (O^{2-}) by deprotonation of H_2O molecules or OH^- ions that are present in the electrolyte [131,133]. The created oxygen anions migrate from the electrolyte/oxide interface across the previously formed oxide layer to reach the metal surface while the Ti^{4+} ions diffuse from the metal surface at the metal/oxide interface towards the oxide/electrolyte interface [139]. Therefore, the growth of the oxide layer described in Equation (4) mainly depends on the ion formation (Ti^{4+} and O^{2-}) process. The interaction between Ti^{4+} and O^{2-} and the diffusion rate of both Ti^{4+} and O^{2-} into the oxide layer is supported by the electrical field. Indeed, the presence of fluoride ions in the electrolyte represents the main key in producing self-organized tubular morphology in the previously formed compact oxide layer. In the main, two reactions are forced by the fluoride ions, the first is a complexation reaction in which they react with the Ti^{4+} cations ejected to the oxide/electrolyte interface to form $[TiF_6]^{2-}$ species as displayed in Equations (6) and (7) [140].

$$Ti^{4+} + 6F^- \rightarrow [TiF_6]^{2-} \quad (6)$$

$$TiO_2 + 6HF^- \rightarrow [TiF_6]^{2-} + 2H_2O + 2H^+ \quad (7)$$

The second reaction is a chemical attack of the compact oxide layer explained in Figure 10.

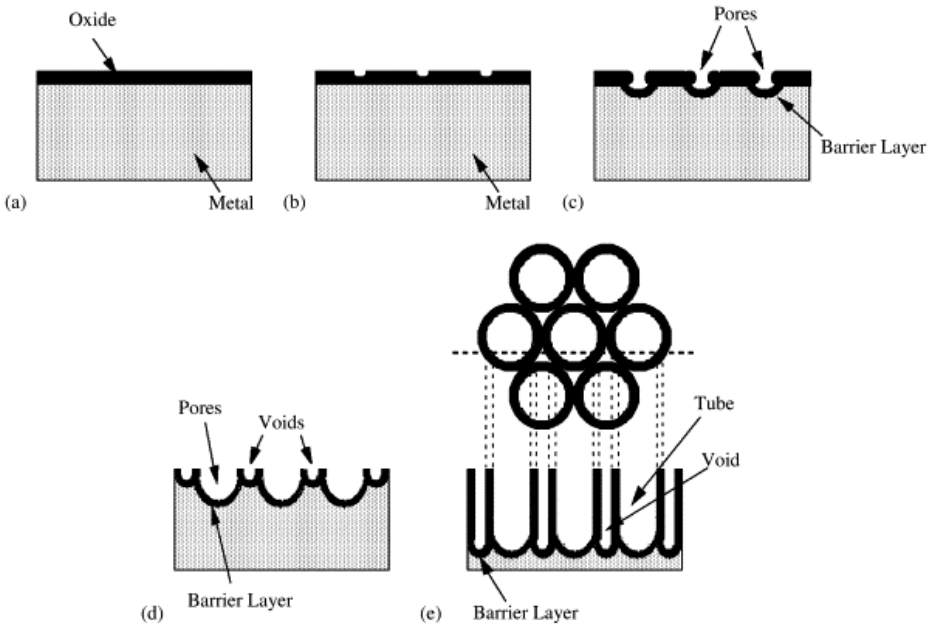

Figure 10. Schematic diagram of the formation mechanism of a nanotube array at constant anodization voltage. (**a**) Compact oxide layer formation, (**b**) pit formation on the oxide layer, (**c**) growth of the pit into scallop shaped pores, (**d**) metallic part between the pores undergoes oxidation and electric field assisted dissolution, and (**e**) fully developed nanotube array with the corresponding top view taken with permission from ref. [126].

Fluoride ions chemically dissolve TiO_2 by forming $[TiF_6]^{2-}$, which is a water soluble species, causing small pits (Equation (6)) [123,138]. These pits represent preferential sites for the electric field assisted chemical dissolution. With time, these pits become deeper and wider and the materials are converted into tubes with the high dissolution rate at these active sites [141]. Therefore, the nanotube heights during the anodization process are controlled by the balance between the rate of electrochemical oxidation and chemical etching. Application of a high anodization voltage leads to an increased electrochemical oxidation compared to the rate of chemical etching. Consequently, a thick layer of TiO_2 nanotubes can be formed before reaching the equilibrium between both rates.

4.5. Anodically Fabricated TiO_2 Nanotubes (NTs) as Potential Anodes in LIBs

As discussed above, the anodic oxidation offers the ability to tune the nanotube dimensions producing well-ordered and high surface area TiO_2 nanotube arrays perpendicularly attached to the Ti substrate. These easily tunable properties open up the possibility for various applications, especially as anodes in lithium ion batteries. The porous nature of such nanotubes can effectively decrease the lithium ion pathway, thus allowing for high lithium ion accessibility of the electrode material [142]. This property, in turn, decreases the polarization of the anode material and triggers a high charging/discharging rate. The high surface area enables intimate contact between the electrode material and the electrolyte causing low charge resistance. Since the formed nanotubes are sized below 20 nm in wall thickness, the one-dimensional structure of the nanotubes is flexible and can buffer volume changes originating from lithium ion insertion and removal.

Systematical studies supported with theoretical analysis were carried out to evaluate the Li ion storage of bare anodically fabricated TiO_2 and the conventional randomly oriented TiO_2 nanotubes mixed mechanically with 10% conductive carbon [143]. The results presented excellent electrochemical performance for the nanotubes prepared by anodization with a six-fold increase in capacity at a current density of 10 C compared to randomly organized TiO_2 nanotubes even after mixing with conductive carbon. These superior performances are ascribed to the good electrical contact between the nanotube

oxide layer and the Ti substrate, which serves as current collector. This arrangement leads to an increased electrical conductivity of the whole electrode [143]. Wei et al. [144] reported the effect of nanotube diameters and wall thicknesses on the storage performance and cycling stability of TiO_2. The nanotubes demonstrated a volumetric capacity of 180 mAh cm^{-3}. The results showed that 96.4% of the initial capacity was retained after 140 cycles for TiO_2 with 50 nm pore diameter and 25 nm wall thickness. When the tube diameter and wall thickness increased to 100 nm and 40 nm, respectively, a rapid capacity fading to only 53% of the original capacity was observed.

In the next sections, various approaches are discussed which affect the electrochemical properties of TiO_2 nanotubes prepared by anodization such as the employed electrolyte, the degree of crystallinity, the annealing atmosphere, structure modifications with carbonaceous materials, post-anodization, and the influence of other transition metal oxides.

4.5.1. Amorphous and Crystalline TiO_2 Anodes

Generally, TiO_2 nanotubes prepared by electrochemical anodization are amorphous. Previous studies showed that the crystalline anatase phase is formed by annealing of the NTs at a temperature above 280 °C in air. At temperatures higher than 450 °C a mixture of well crystalline anatase and small amounts of rutile are obtained [127]. A temperature between 600 to 900 °C is required for the complete phase transition from anatase to rutile [47,145]. Other studies showed that single-phase anatase is obtained after annealing of mixed or coated TiO_2 nanotubes at 450 °C. Nevertheless, the crystallization process of the NT depends on the specific chemical composition of the used metal and on the local diffusion of the alloying element. For example, Nb increases the conversion temperature of anatase to rutile [146]. Hence, rutile is not formed in the grown nanotubes on Ti6Al7Nb even when they are annealed at 550 °C. Alternatively, Fe concentration in a Ti-Fe alloy can promote the formation of rutile and decrease the anatase phase [147].

Particular interest was paid to investigate the relation between the degree of crystallinity and the electrochemical performance of TiO_2 nanotubes as anodes for lithium ion batteries. Experiments were conducted by Ivanov et al. [148] which revealed that the amorphous TiO_2 structure promotes a higher lithium ion diffusion rate than the crystalline anatase structure. The reason was attributed to larger amount of disorders and defects in the amorphous state than in the crystalline one. These defects offer bigger channels or more diffusion paths for Li ion migration. In addition, the low mechanical stress and less rigid nature owned by amorphous TiO_2 facilitate intercalation in large amounts [145,149]. Furthermore, Ryu et al. [150] reported a comparative study of amorphous vs. crystalline TiO_2 NTs and their storage capacity, rate capability, and cycling stability. The as-prepared and post-annealing NTs showed similar pore diameters (30–50 nm) and tube heights (8.2 μm). The voltage profiles of the amorphous tubes reach much higher specific capacities than the crystalline TiO_2 (Figure 11) due to the higher Li ion diffusivity in the amorphous structure. The rate capability of amorphous and crystalline anatase NTs was investigated by Fang et al. [151]. Amorphous TiO_2 exhibited a high rate capability compared to crystalline anatase fabricated with the same morphological features. This phenomenon is proven by the higher Li ions diffusion coefficient of amorphous TiO_2 compared to anatase.

Tighineanu et al. [152] studied the influence of annealing temperature and time on the ionic conductivity of TiO_2 nanotube arrays. The ionic conductivity of TiO_2 mainly depends on the conversion process from amorphous TiO_2 to the crystalline phases, where anatase showed a higher electrical conductivity than rutile-containing tube arrays. The optimal annealing temperature to obtain low resistance materials was found to be between 250 and 450 °C. This work also showed that crystalline anatase is obtained by annealing amorphous TiO_2 at 250 °C for a longer time up to 20 h [152]. Mixed compositions of anatase and rutile in the TiO_2 nanotube arrays, after thermal treatment above 580 °C, demonstrated higher areal capacity than that achieved by single anatase NTs [153]. The authors associated the enhanced insertion capacity with the higher Li ion diffusion coefficient of rutile in playing a stronger role than the improved electrical conductivity of anatase.

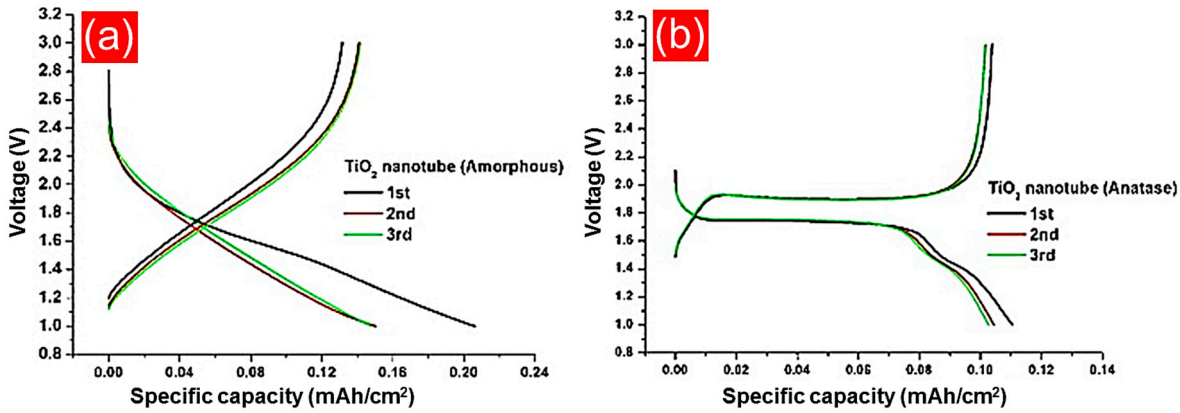

Figure 11. Voltage profiles of (**a**) amorphous TiO_2 and (**b**) anatase nanotubes measured at a current density of 100 μA cm^{-2}. Adapted with permission from ref. [150].

4.5.2. Anodization Electrolyte

Ionic liquids as anodization bath were explored in different reports to produce defect-free TiO_2 nanotubes with good mechanical strength to improve the charge transfer efficiency. These electrolytes are characterized by higher electrical conductivity which helps to decrease the decomposition of the electrolyte during the anodization process. However, the TiO_2 nanotubes fabricated with liquid ionic electrolytes showed a good cycling stability for more than 1000 cycles. The obtained reversible capacity is relatively low (~140 mAh g^{-1}) at a low charging rate (0.1 C) [146].

4.5.3. Influence of the Annealing Atmosphere on the Properties of TiO_2 Nanotube Anodes

Considerable attention has been drawn to the annealing atmosphere of the TiO_2 nanotubes as an important factor for their electrochemical storage properties. Experiments explored how the annealing atmosphere can affect the morphology and the present crystalline phases of the nanotube arrays. Free-standing TiO_2 nanotubes annealed in Ar atmosphere showed morphological features which differ from those obtained during annealing in air as presented in Figure 12a,b [154]. Furthermore, the electrochemical tests showed better performances for the sample annealed in Ar compared to that annealed in air (Figure 12c).

This behavior was explained by the presence of significant amounts of carbon mixed with the thermally treated nanotubes leading to improved electrical conductivity. Enhanced initial lithium ion insertion capacity up to 240 mAh g^{-1} at a current density of 320 mA g^{-1} was reported by Liu et al. [155] for anatase nanotube arrays when they were annealed in a N_2 atmosphere at 300 °C.

The achieved capacity decreased as the annealing temperature increased. The authors correlated their observation to the lower storage ability of rutile obtained by phase transformation from anatase at high temperatures leading to a reduced overall electrode capacity. Lu et al. [156] investigated the use of H_2/95% Ar as a reducing atmosphere to thermally treat the anodized TiO_2 NTs. Structural and morphological changes were observed for the annealed nanotubes in this reducing atmosphere associated with an improvement in their electrochemical rate performance during lithium insertion measurements. Results of the detailed experiments indicate the hydrogen treatment produced a large number of oxygen vacancies inside the crystal lattice of TiO_2, which represents active sites for Li ions diffusion and intercalation [156].

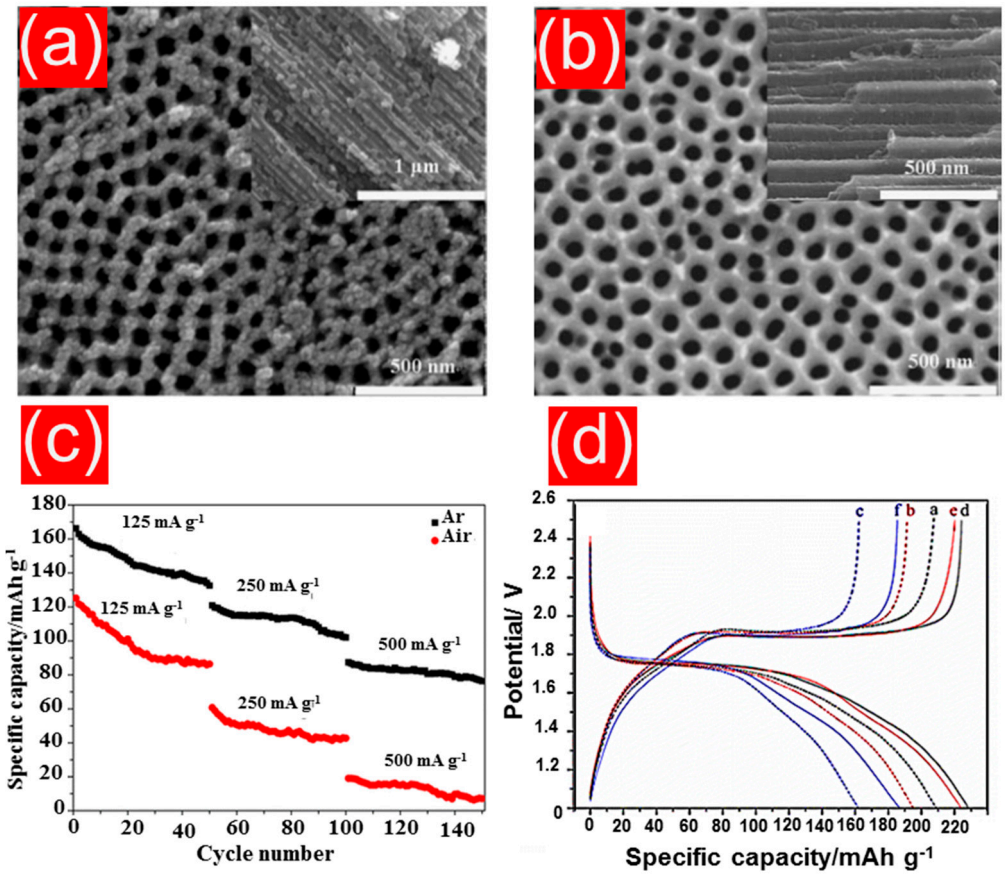

Figure 12. SEM micrographs of the TiO_2 nanotubes thermally treated in (**a**) Ar in (**b**) air atmosphere and (**c**) the rate capability of each electrode, (**d**) voltage profile curves of the first discharge cycle of TiO_2 membranes, a, b, c representing annealed at 450 °C, 600 °C, and 800 °C in air, with d, e, f being 450 °C, 600 °C, 800 °C in Ar, respectively. Adapted with permission from ref. [154].

4.5.4. Free-Standing TiO_2 Nanotube Membranes

In addition to the nanotubes grown on Ti foils, there is great interest in using the TiO_2 nanotube membranes after the detachment from the substrates, especially when they can be used in applications like microbatteries. Wei et al. [157] reported a two-step anodization process followed by a thermal treatment to fabricate TiO_2 nanotube films. The TiO_2 membranes were separated from the Ti substrates by sonication. The resulting 3D free-standing TiO_2 nanotube layers were evaluated as anodes for microbatteries and exhibited an areal capacity of 0.46 mA cm^{-2} (i.e., 184 mAh g^{-1}) at a current density of 0.05 mA cm^{-2}. Furthermore, these membrane electrodes demonstrated excellent cycling stability over 500 cycles with an overall capacity loss of about 6%. The found areal capacity depends on the nanotube length. Interestingly, by using two anodization steps, TiO_2 nanotubes with small pore diameter are formed. This aspect was utilized by Liu et al. [158] to produce nanotubes of 20 nm in length which showed excellently enhanced electron transport.

The above-mentioned approaches were aimed at increasing lithium ion storage performance by optimizing the nanotube dimensions, annealing temperature, and the environment to reduce the internal resistivity of the TiO_2 materials, but the poor electrical conductivity needs to be improved. Doping or coating TiO_2 nanotubes with other materials which are more conductive, such as graphene or CNTs, is usually the general protocol to overcome the conductivity obstacles.

4.5.5. TiO_2 Nanotubes/Carbon Composites

Similar to TiO_2 nanoparticles and nanowires, doping of TiO_2 nanotubes with highly conductive materials were explored. Here, the aim was to improve the electronic conductivity of TiO_2 using carbon composites which provide more electrons to the TiO_2 surface to achieve a higher Li ion storage at very fast charging/discharging rates. Kilinic et al. [159] succeeded in fabricating C-doped TiO_2 nanotubes grown on Ti foils by anodic oxidation. Doping was performed through two different methods. The first is an in-situ synthesis during the anodic oxidation process. The key point here is the anodic oxidation electrolyte which must contain a carbon source such as polyvinyl alcohol. The second is a heat treatment method in which the anodized TiO_2 nanotubes are subjected to a thermal treatment at 500 °C under a N_2/C_2H_2 flux (1:1). Furthermore, carbon-modified anodically prepared TiO_2 nanotubes were also investigated by Mole et al. [160] by thermal treatment in a CH_4/H_2 atmosphere in the presence of Fe. A threefold increase in the double layer capacitance was demonstrated by C-TiO_2 nanotubes compared to the pure TiO_2 nanotube electrodes due to the improved charge transfer obtained by the presence of carbon and iron dopants. In addition, Chen et al. [161] developed a simple method to fabricate Au/RGO-TiO_2 NT composites via electrolysis of chloro-auric acid and graphene oxide on the surface of anodically fabricated TiO_2 nanotubes. These composite materials were only tested as photocatalysts. Fabrication of binary CNTs@TiO_2 composite anodes was recently studied by Madian et al. [162]. They synthesized a network of multiwalled CNTs laterally deposited onto the surface of anodically grown TiO_2 using a simple spray pyrolysis technique (Figure 13a,b). The CNTs@TiO_2 composite electrodes showed enhanced electrochemical performances over a current density range between 50 and 500 μA cm^{-2} exhibiting a 1.5-fold increase in the areal capacity compared to pure thermally treated and untreated TiO_2 anodes (Figure 13c). The noticed electrochemical performance was ascribed to the improved charge transport and electronic conductivity of the composite anode due to the presence of a highly conductive network of CNTs that interfaced the TiO_2 NT. In addition, this tightly interwoven network can function as a second charge collector. In such studies, similar improvement in the electrochemical performance was observed for the CNT-coated TiO_2-CoO NTs compared to the mixed TiO_2-CoO NT.

4.5.6. Mixed Oxide Nanotubes

The fabrication of ordered mixed transition metal oxide nanotubes is usually obtained by two approaches, the first includes more than one preparation step in which the nanotubes are first fabricated via the usual synthesis procedures discussed above (such as anodization or atomic layer deposition) and are subsequently subjected to doping or coating processes. The second approach is realized by a single preparation step in which Ti-based alloys are used as substrates for the anodization to directly form mixed oxide tubes onto the surface. For instance, Co_3O_4 nanoparticles@TiO_2 nanotubes were synthesized by the electrodeposition of Co_3O_4 onto the grown TiO_2 nanotubes (Figure 14a). The Co_3O_4@TiO_2 composite was explored for lithium ion storage [163]. The coated Co_3O_4 layer leads to an increase of the Li ion insertion capacity which is related to the improved ionic conductivity as well as contributing to the overall electrode capacity itself. An interesting in-situ preparation process during the anodization of Ti foils was reported by Cao et al. [164] to produce Co_3O_4-doped TiO_2 nanotubes in which $Co(NO_3)_2 \cdot 6H_2O$ was utilized as cobalt source in the anodic oxidation electrolyte. This composite material showed enhanced photoelectrochemical properties under visible light but no results concerning energy storage applications were reported. Self-doping and electrodeposition techniques were employed to achieve uniform copper filling from the bottom to the top of the TiO_2 nanotubes [165]. That strategy was proposed to enhance the conductivity of the tube bottoms using a conductive copper coating. Similar to copper-filled TiO_2 nanotubes, α-Fe_2O_3 was selected and prepared by a pulse electrodeposition to finally form Fe_2O_3 nanorod/TiO_2 nanotube composites [166]. This approach allows for the growing of Fe_2O_3 rods with various lengths ranging between 50 and 550 nm according to the deposition time. In another study, Fe_2O_3 hollow nanorods were formed

on the outer and inner surface of anodically fabricated TiO_2 to prepare 3D hierarchical structures of Fe_2O_3@TiO_2 [167].

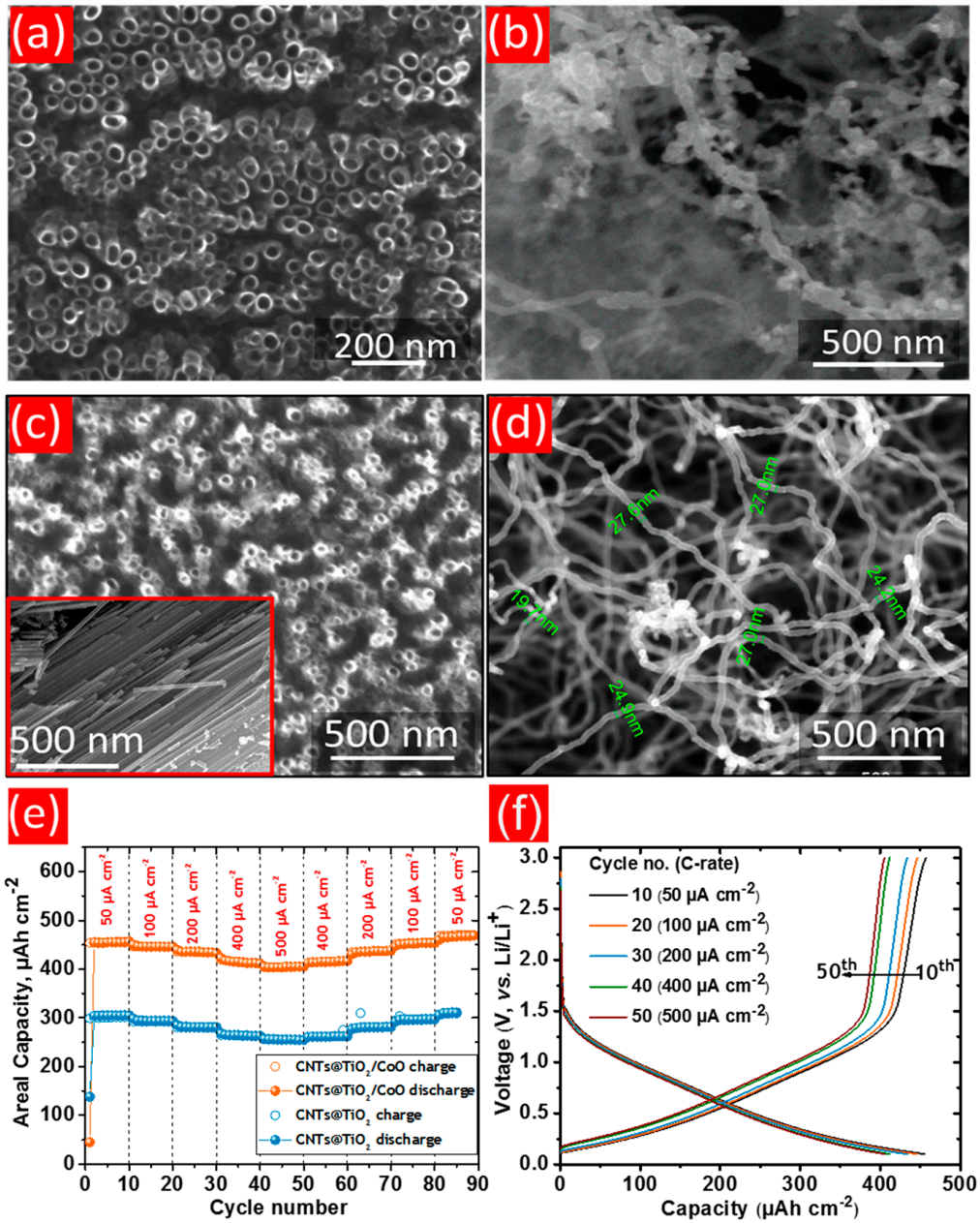

Figure 13. SEM micrographs of uncovered (**a**) TiO_2 nanotubes, (**b**) CNTs@TiO_2 composite, (**c**) TiO_2-CoO NT, (**d**) CNTs@TiO_2-CoO NT. (**e**) The electrochemical performance of CNTs@TiO_2 and CNTs@TiO_2-CoO composite electrodes, (**f**) typical voltage profiles for the 10th, 20th, 30th, 40th, and 50th cycles against areal capacity of TiO_2-CoO NT anodes, adapted with permission from ref. [162].

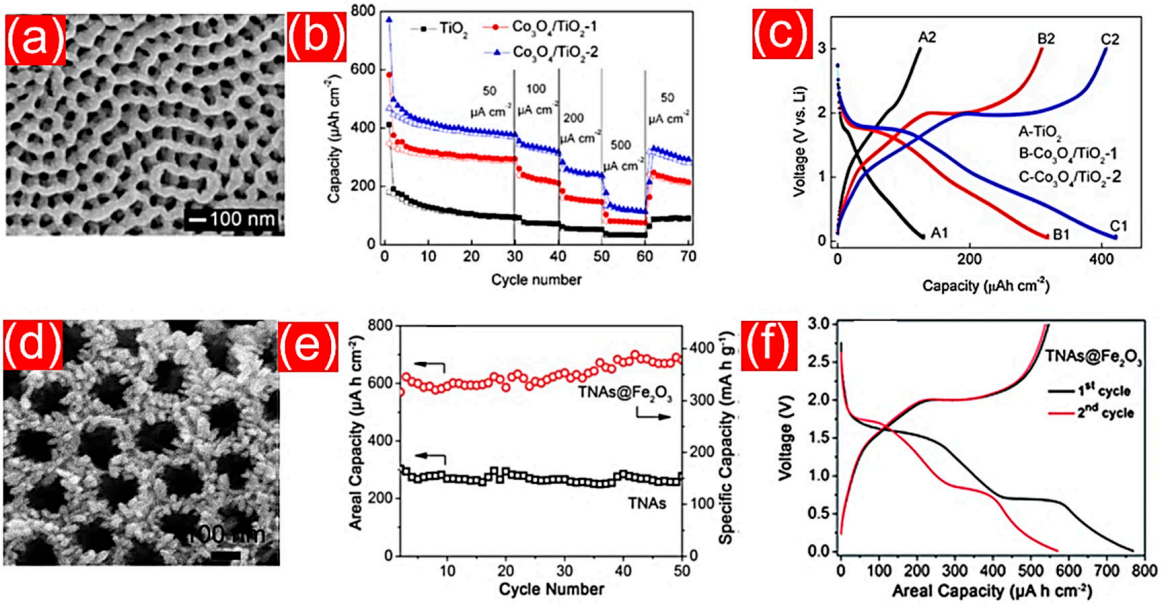

Figure 14. (**a**) SEM images of Co_3O_4-coated TiO_2 nanotubes obtained at photodeposition time of 4 h and (**b**) their areal capacities measured at different current densities, (**c**) voltage profile curves of bare TiO_2 (A), as-synthesized Co_3O_4/TiO_2-1 with Co_3O_4 loading of 0.12 mg cm^{-2} (B) and Co_3O_4/TiO_2-2 with Co_3O_4 loading of 0.25 mg cm^{-2} (C) electrodes as anodes in the 10th cycle adapted from ref. [163]. (**d**) SEM image of Fe_2O_3 nanorod onTiO_2. (**e**) Cycling performances of Fe_2O_3@TiO_2 in comparison with bare TiO_2 and (**f**) their voltage profile in the 1st and 2nd cycles. Adapted with permission from ref. [167].

The preparation technique includes the hydrolysis of Fe^{3+} ions to grow FeOOH nanospindles followed by the thermal transformation to Fe_2O_3 nanorods as presented in Figure 14d,e. This heterojunctional composite was integrated as electrode in an LIB and demonstrated an outstanding electrochemical performance with an areal capacity of about 600 μA cm^{-2} that was retained for 50 cycles at a current density of 100 μA cm^{-2} (Figure 14f). Homogenous VO_x nanoparticles were also deposited onto TiO_2 nanotube arrays by chemical vapor deposition. The well-dispersed VO_x particles on the nanotube surface make TiO_2 a highly attractive catalytic material for different reactions [168]. Guan et al. [169] reported an easily controllable synthesis of MoO_3-doped TiO_2 nanotube arrays via anodic oxidation followed by the electrodeposition of MoO_3. The MoO_3-modified nanotube electrodes were able to deliver twice the areal capacity of bare TiO_2. However, the electrochemical impedance spectra (EIS) analysis demonstrated that the Li ion transfer into TiO_2 is blocked by a thick layer of deposited MoO_3 nanoparticles. Therefore, the contribution of MoO_3 nanoparticles to the insertion capacity of the whole electrode was ascribed as a possible reason for the increased capacity. Gobal et al. [170] investigated the electrodeposition of Zn-Ni onto TiO_2 nanotubes in alkaline solution subsequently after thermal annealing at 300 °C to form NiO-ZnO/TiO_2 nanoporous but partially cracked composites. The assembled electrodes demonstrated good capacitive behavior as supercapacitor and were not tested as a Li ion battery.

To strengthen the anodic behavior of TiO_2 NTs, SnO_2 nanowires were grown on the surface of TiO_2 NTs by a two-step method in which the previously anodized TiO_2 nanotubes were subjected to an electrodeposition process. Sn and SnO_2 present in the mixed oxide electrodes were tested for Li ion storage by limiting the voltage ranges to 1.2–0.01 V vs. Li^+/Li [171]. An areal capacity of 140 μAh cm^{-2} was demonstrated by a 2 μm thick Sn/SnO_2 layer with a capacity retention of up to 85% after 50 cycles. The TiO_2 NTs helped to buffer the volume changes of the Li-Sn alloys and, thus, improved the overall electrode performance [171]. SnO_2 deposited coaxially onto TiO_2 nanotubes were synthesized by post electrodeposition and the corresponding SEM image is presented

in Figure 15a [172]. The prepared monohybrids displayed a good electrical conductivity and, thus, an enhanced electrochemical performance for Li ion storage (Figure 15b). As previously mentioned template-assisted atomic layer deposition (ALD) is considered as an alternative technique to fabricate TiO_2 with controlled tubular geometry but expensive infrastructure and growth time may limit this approach. Kim et al. [173] reported on the fabrication of SnO_2/TiO_2 NT heterostructures by ALD. The resulting mixed oxide electrodes offer a specific capacity of 100 mAh g^{-1} in the second cycle. However, a capacity of 300 mAh g^{-1} was maintained by this electrode even after 50 cycles. The surface modification by SnO_2 was designated to enhance the lithium insertion rate and, thus, increased the specific capacity of such electrode composite compared to pure TiO_2 (250 mAh g^{-1}).

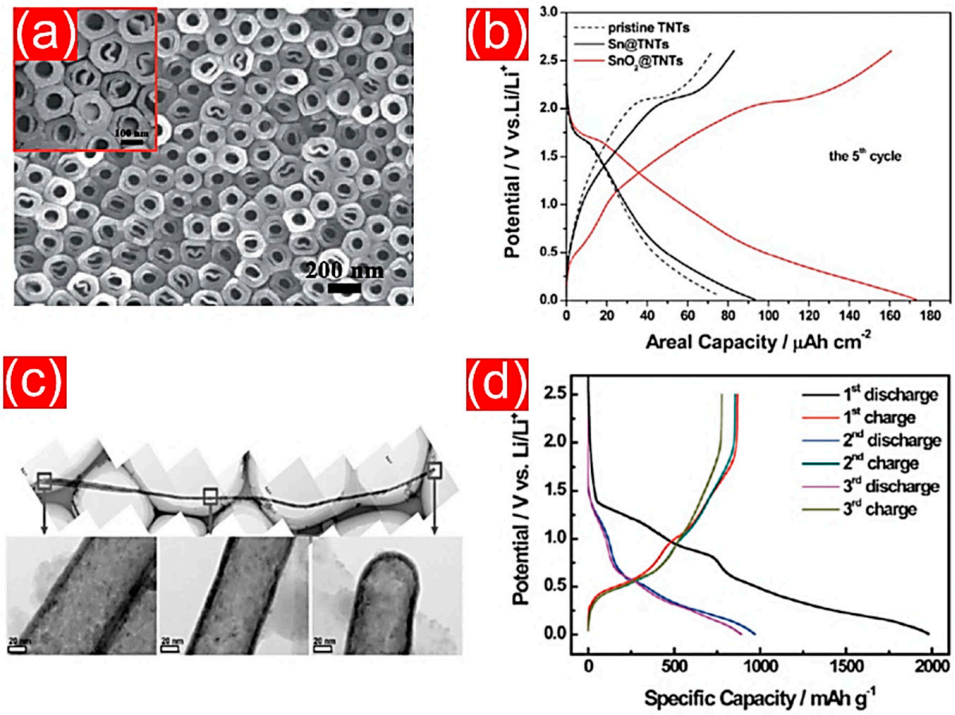

Figure 15. (**a**) SEM image of coaxial $SnO_2@TiO_2$ nanotubes synthesized by post electrodeposition. (**b**) Their galvanostatic charging-discharging curves obtained at a current rate of 100 μA cm^{-2}, adapted from ref. [172]. TEM images of an atomic layer deposition (ALD)-grown SnO_2. (**c**) The magnified images obtained from three different regions are presented as insets with (**d**) galvanostatic charging-discharging curves measured at a current rate of 0.1 C, adapted with permission from ref. [173].

Surface modification to TiO_2 nanotubes can also be carried out by deposition of Li_3PO_4 on the surface as presented by Lopez et al. [174]. The obtained 3D structure of Li_3PO_4-coated TiO_2 was assembled as electrode and was tested for lithium ion storage. The electrochemical results revealed a reversible capacity of 110 mAh g^{-1} achieved for over 190 cycles at a rate of 5 C. The lithium phosphate was proposed in that composite as ionic conductor which improved the electrical and ionic conductivity of TiO_2 [174]. Alternatively, a straightforward approach used to fabricate self-organized mixed oxide nanotube arrays is found in the anodic oxidation of Ti-based alloys.

Although several binary and ternary mixed oxide nanotubes were fabricated by the anodization of Ti-Fe [148], Ti-Ta, Ti-Nb [175], Ti-Pd [176], Ti-Al [177], Ti-Mo [178], Ti-V [179], Ti-W [180], Ti-Mn [181], Ti-Ni [182], Ti-Mo-Ni [183], and Ti-6Al-4V [184] alloys, only some of them were applied as electrodes in lithium ion batteries. As an example, well-ordered mixed Ti-Mn-O nanotubes were grown on the surface of a Ti-8Mn alloy by anodization [181]. The mixed oxide anodes were integrated with a $LiCoO_2$ cathode to assemble a full cell battery. These mixed oxide nanotubes showed a capacity of 474 mAh g^{-1} which was held for 30 cycles. A decent electrode of ordered TiO_2/Nb_2O_5 nanotubes

demonstrated long-term cycling stability and higher reversible lithium storage capacity than pure TiO_2 nanotube arrays prepared under similar conditions [185]. Madian et al. [125] showed the ability to fabricate self-ordered CoO/TiO_2 NTs by the anodic oxidation of two-phase Ti-Co alloy, as presented in Figure 16. This hybrid oxide anode was synthesized at 60 V, and demonstrated an areal capacity of 600 μAh cm^{-2} corresponding to 315 mAh g^{-1} at a current density of 10 μA cm^{-2} with a Coulombic efficiency of 96%. Such electrodes showed a 1.6 increase in the capacity compared to pure TiO_2 NT synthesized under the same conditions preserving 88% of their initial capacity over 100 cycles.

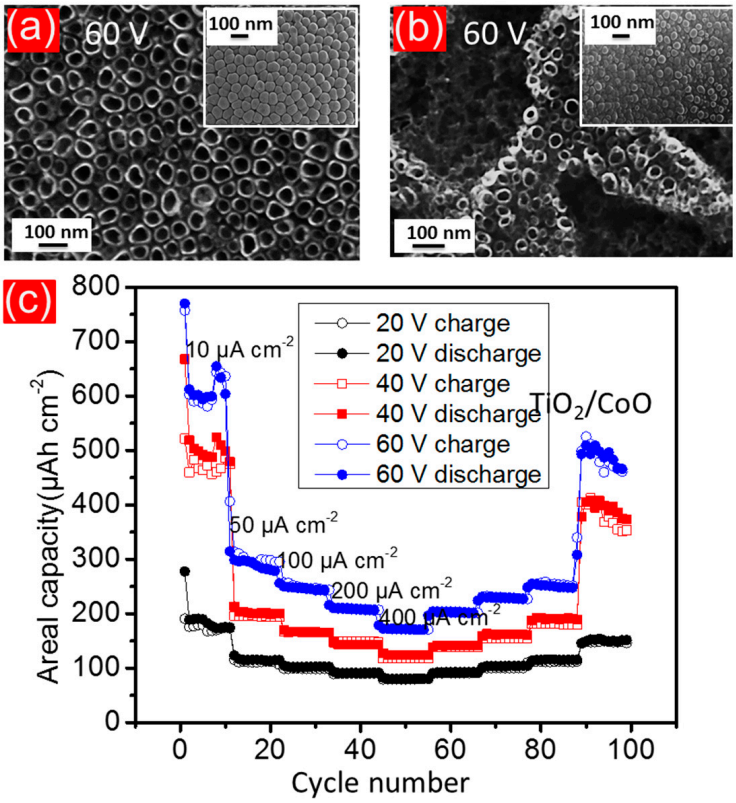

Figure 16. (**a**) SEM images of the Ti−Co alloy anodized at 60 V with the β-Ti phase, and (**b**) the Ti_2Co phase. (**c**) Rate capability of TiO_2/CoO, prepared at anodization voltages of 20 V (black circles), 40 V (red squares) and 60 V (blue circles), as a function of cycle number. The filled symbols relate to the discharging and open symbols to the charging processes. Adapted with permission from ref. [125].

Madian et al. [186] worked on the improvement of TiO_2 NT arrays for potential anode application with single phase Ti-Sn alloys. Different Sn concentrations (1–10 at %) were utilized to grow well-organized Ti-Sn-O NT. The as-prepared nanotubes on a $TiSn_1$ alloy at 40 V (Figure 17a,b) exhibited an areal capacity of 405 μAh cm^{-2} (i.e., 212 mAh g^{-1}) at a current density of 504 μA cm^{-2} with a superior cycling stability over 400 cycles as shown in Figure 17c. A 1.4 times higher capacity was demonstrated by these mixed oxide electrodes compared to the pure TiO_2 NT fabricated under similar conditions. This effect was attributed to the high surface area and the improved ionic conductivity due to the presence of SnO_2 NTs on the $(TiSn)O_2$ NTs, resulting in a higher lithium ion diffusion rate. The tubular structure of the mixed oxide electrodes remained unaffected over the electrochemical cycling.

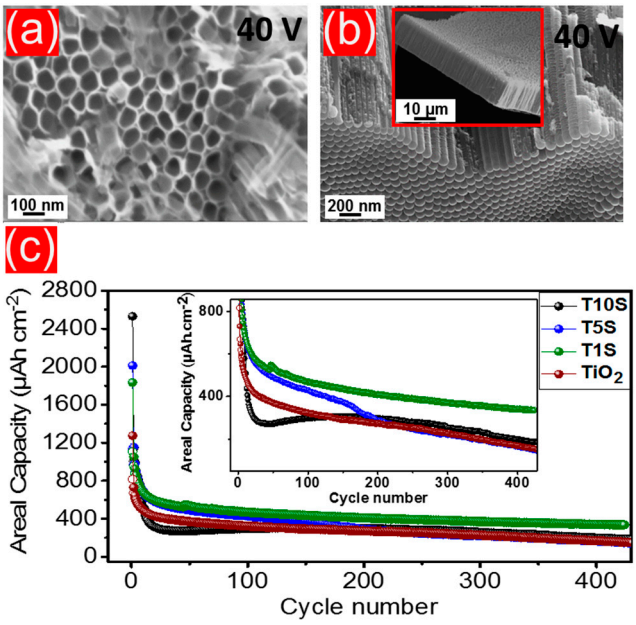

Figure 17. (**a**) SEM micrographs of the $TiSn_1$ alloy anodized at 40 V for 5 h; (**b**) Cross-sectional view of the nanotubes grown at 40 V. The inset in (b) shows the uniform growth of the nanotubes. (**c**) Galvanostatic cycling obtained at a current density of 504 mA cm^{-2} for pure TiO_2 (dark red circles) and TiO_2/SnO_2 anodes. T1S (green circles), T5S (blue circles), and T10S (black circles) correspond to the nanotubes prepared on the $TiSn_1$, $TiSn_5$, and $TiSn_{10}$ alloy substrates, respectively, adapted with permission from ref. [186].

5. Summary

An enormous number of studies have investigated the synthesis and modifications of TiO_2-based nanostructured electrodes to look for improved electrochemical performance when applied to lithium ion batteries. Table 2 summarizes the most promising electrochemical results on TiO_2 nanostructures based anodes. TiO_2 NT arrays are one group of nanostructures which basically offer high structural stability and safety during cycling, as these are crucial requirements in many proposed applications, i.e., medical and defense sector. On taking a deep look into the state-of-the-art, two main questions need to be discussed: (I) How can the improvement of the ionic and electrical conductivities be realized to result in better lithium insertion characteristics? (II) How is an increase in specific capacity possible in order to meet the requirements of proposed applications? Optimizing the size and morphology of TiO_2 nanostructures with new synthesis technologies has been shown to be an effective strategy to reduce the lithium ion diffusion pathway and electrolyte decomposition leading to high Coulombic efficiency. TiO_2 composite with high lithium storage capacity and/or high electronic conductivities is an ideal route to obtain high power and high energy density anodes for safe application. Meanwhile, the criteria of easy manufacturing and low cost have to be fulfilled in future research and especially in up-scaling attempts in order to meet the market requirements. The fabrication of self-organized and highly ordered TiO_2 nanotubes by anodic oxidation has been extensively addressed here because this technique may possibly reach all the previously defined property and market criteria. Additionally, critical aspects affecting the electrochemical performance of the anodically prepared TiO_2 nanotubes are highlighted. These aspects include the formation mechanism, the impact of morphology, crystallinity, annealing atmosphere and temperature, surface modification with carbonaceous materials, and mixing with other transition metal oxides. Moreover, we pointed out the recent methods used to synthesize mixed oxide nanotubes, either with two-step or single-step preparation methods. In short, this report is designated to guide and help the science in this field to overcome the challenges presented above and to give nanostructured TiO_2 oxide systems a real chance for a broad application.

Table 2. Electrochemical performance of various TiO_2 nanostructure based anodes.

Composition	Synthesis	Capacity after 20th Cycle	Current Rate	Number of Reversible Cycles	Reference
Rutile nanoparticles	Commercially obtained	207 mAh g^{-1}	0.05 A g^{-1}	20	[65]
Anatase nanoparticles	solvothermal	196 mAh g^{-1}	0.2 C	100	[69]
TiO_2@C hollow spheres	sol-gel hydrothermal	170 mAh g^{-1}	2 C	300	[72]
TiO_2 nanoparticles@graphene	in-situ hydrolysis	70 mAh g^{-1}	5 A g^{-1}	400	[75]
Core-shell CNTs/TiO_2	hydrolysis	240 mAh g^{-1}	5 A g^{-1}	100	[74]
Anatase nanorods	hydrolysis	206 mAh g^{-1}	50 mA g^{-1}	30	[90]
Anatase nanowires	hydrolysis	280 mAh g^{-1}	140 mA g^{-1}	40	[92]
TiO_2 nanofibers	electrospinning	170 mAh g^{-1}	0.3 C	50	[95]
C-doped TiO_2 nanowires	hydrothermal	306 mAh g^{-1}	0.1 C	1000	[96]
TiO_2 NT@graphene	hydrothermal	357 mAh g^{-1}	10 mA g^{-1}	50	[98]
TiO_2/C hollow nanofibers	force spinning	229 mAh g^{-1}	100 mA g^{-1}	100	[100]
Graphene-wrapped TiO_2 nanofibers	electrospinning	200 mAh g^{-1}	0.1 C	35	[101]
Anatase/graphene nanosheets	solvothermal	161 mAh g^{-1}	1 C	120	[102]
TiO_2/graphene	hydrolysis	230 mAh g^{-1}	0.1 C	100	[103]
TiO_2 nanoporous hollow spheres	template-assisted	230 mAh g^{-1}	33.5 mA g^{-1}	50	[106]
Mesoporous TiO_2 nanoparticles	template-assisted	268 mAh g^{-1}	0.2 C	30	[107]
C-coated mesoporous TiO_2@graphene sheets	solvothermal	111 mAh g^{-1}	0.2 A g^{-1}	100	[109]
Fe_2O_3 nanorods-TiO_2	thermal treatments	860 mAh g^{-1}	1 A g^{-1}	1000	[112]
Hierarchical TiO_2/Fe_2O_3 fiber-in-tube	electrospinning	987 mAh g^{-1}	100 mA g^{-1}	240	[113]
Hierarchically ordered porous anatase	chemical etching	191 mAh g^{-1}	1 A g^{-1}	60	[115]
Hierarchical nanosheets	solvothermal alcoholysis	225 mAh g^{-1}	1 C	700	[118]
TiO_2 NTs	anodization	140 mAh g^{-1}	0.1 C	1000	[145]
3D free-standing TiO_2 NTs	anodization	184 mAh g^{-1}	0.05 mA cm^{-2}	500	[157]
SnO_2/TiO_2 NTs	atomic layer deposition	250 mAh g^{-1}	0.1 C	50	[173]
Ti-Mn-O NTs	anodization	474 mAh g^{-1}	175 mA g^{-1}	30	[181]
CoO/TiO_2 NTs	anodization	600 μAh cm^{-2}	10 μA cm^{-2}	100	[125]
TiO_2-SnO_2 NTs	anodization	405 μAh cm^{-2}	504 μA cm^{-2}	400	[186]
CoO/TiO_2NTs	anodization—chemical vapor deposition	450 μAh cm^{-2}	50 μA cm^{-2}	90	[156]

Acknowledgments: Financial support was received partially by the European Union and the Free State of Saxony (SAB grant no. 100225299) as well as the German Federal Ministry of Research and Education through the project ADNAMSES (grant no. 01DH14002) and is gratefully acknowledged.

Author Contributions: Mahmoud Madian conceptualized and wrote the main manuscript. Lars Giebeler contributed in writing, discussed and edited the text. Alexander Eychmüller contributed to scientific discussion and edited the manuscript.

Conflicts of Interest: The authors declare no conflict of interest.

References

1. Broussely, M.; Biensan, P.; Simon, B. Lithium insertion into host materials: The key to success for Li ion batteries. *Electrochim. Acta* **1999**, *45*, 3–22. [CrossRef]
2. Nishi, Y. Lithium ion secondary batteries; past 10 years and the future. *J. Power Sources* **2001**, *100*, 101–106. [CrossRef]
3. Aldissi, M. Multi-layered polymer electrolytes towards interfacial stability in lithium ion batteries. *J. Power Sources* **2001**, *94*, 219–224. [CrossRef]
4. Wen, J.; Yu, Y.; Chen, C. A review on lithium-ion batteries safety issues: Existing problems and possible solutions. *Mater. Express* **2012**, *2*, 197–212. [CrossRef]
5. Uhlmann, C.; Illig, J.; Ender, M.; Schuster, R.; Ivers-Tiffée, E. In situ detection of lithium metal plating on graphite in experimental cells. *J. Power Sources* **2015**, *279*, 428–438. [CrossRef]
6. Bandhauer, T.M.; Garimella, S.; Fuller, T.F. A critical review of thermal issues in lithium-ion batteries. *J. Electrochem. Soc.* **2011**, *158*, R1–R25. [CrossRef]
7. Yaakov, D.; Gofer, Y.; Aurbach, D.; Halalay, I.C. On the study of electrolyte solutions for Li-ion batteries that can work over a wide temperature range. *J. Electrochem. Soc.* **2010**, *157*, A1383–A1391. [CrossRef]
8. Yariv, O.; Hirshberg, D.; Zinigrad, E.; Meitav, A.; Aurbach, D.; Jiang, M.; Powell, B.R. Carbon Negative Electrodes for Li-Ion Batteries: The effect of solutions and temperatures. *J. Electrochem. Soc.* **2014**, *161*, A1422–A1431. [CrossRef]

9. Rodrigues, M.-T.F.; Babu, G.; Gullapalli, H.; Kalaga, K.; Sayed, F.N.; Kato, K.; Joyner, J.; Ajayan, P.M. A materials perspective on Li-ion batteries at extreme temperatures. *Nat. Energy* **2017**, *2*, 17108. [CrossRef]
10. Xu, L.; Kim, C.; Shukla, A.K.; Dong, A.; Mattox, T.M.; Milliron, D.J.; Cabana, J. Monodisperse Sn nanocrystals as a platform for the study of mechanical damage during electrochemical reactions with Li. *Nano Lett.* **2013**, *13*, 1800–1805. [CrossRef] [PubMed]
11. Wen, C.J.; Boukamp, B.A.; Huggins, R.A.; Weppner, W. Thermodynamic and mass transport properties of "LiAl". *J. Electrochem. Soc.* **1979**, *126*, 2258–2266. [CrossRef]
12. Saint, J.; Morcrette, M.; Larcher, D.; Tarascon, J.M. Exploring the Li-Ga room temperature phase diagram and the electrochemical performances of the Li_xGa_y alloys vs. Li. *Solid State Ion.* **2005**, *176*, 189–197. [CrossRef]
13. Yoon, S.; Park, C.M.; Sohn, H.J. Electrochemical characterizations of germanium and carbon-coated germanium composite anode for lithium-ion batteries. *Electrochem. Solid State Lett.* **2008**, *11*, A42–A45. [CrossRef]
14. Martos, M.; Morales, J.; Sánchez, L. Lead-based systems as suitable anode materials for Li-ion batteries. *Electrochim. Acta* **2003**, *48*, 615–621. [CrossRef]
15. Dailly, A.; Ghanbaja, J.; Willmann, P.; Billaud, D. Lithium insertion into new graphite-antimony composites. *Electrochim. Acta* **2003**, *48*, 977–984. [CrossRef]
16. Li, H.; Li, H.; Huang, X.; Huang, X.; Chen, L.; Chen, L.; Wu, Z.; Wu, Z.; Liang, Y.; Liang, Y. A high capacity nano-Si composite anode material for lithium rechargeable batteries. *Electrochem. Solid State Lett.* **1999**, *2*, 547–549. [CrossRef]
17. Cao, F.F.; Deng, J.W.; Xin, S.; Ji, H.X.; Schmidt, O.G.; Wan, L.J.; Guo, Y.G. Cu-Si nanocable arrays as high-rate anode materials for lithium-ion batteries. *Adv. Mater.* **2011**, *23*, 4415–4420. [CrossRef] [PubMed]
18. Fan, X.; Zhang, H.; Du, N.; Wu, P.; Xu, X.; Li, Y.; Yang, D. Vertically ordered Ni_3Si_2/Si nanorod arrays as anode materials for high-performance Li-ion batteries. *Nanoscale* **2012**, *4*, 5343–5347. [CrossRef] [PubMed]
19. Ji, L.; Lin, Z.; Alcoutlabi, M.; Zhang, X. Recent developments in nanostructured anode materials for rechargeable lithium-ion batteries. *Energy Environ. Sci.* **2011**, *4*, 2682–2699. [CrossRef]
20. Liu, Y.; Yang, Y. Recent progress of TiO_2-based anodes for Li ion batteries. *J. Nanomater.* **2016**, *2016*, 8123652. [CrossRef]
21. Agubra, V.A.; Zuniga, L.; Flores, D.; Villareal, J.; Alcoutlabi, M. Composite nanofibers as advanced materials for Li-ion, Li-O_2 and Li-S batteries. *Electrochim. Acta* **2016**, *192*, 529–550. [CrossRef]
22. Agubra, V.A.; Zuniga, L.; Flores, D.; Campos, H.; Villarreal, J.; Alcoutlabi, M. A comparative study on the performance of binary SnO_2/NiO/C and Sn/C composite nanofibers as alternative anode materials for lithium ion. *Electrochim. Acta* **2017**, *224*, 608–621. [CrossRef]
23. Ji, L.; Meduri, P.; Agubra, V.; Xiao, X.; Alcoutlabi, M. Graphene-based nanocomposites for energy storage. *Adv. Energy Mater.* **2016**, *6*, 1502159. [CrossRef]
24. Wagemaker, M.; Kearley, G.J.; van Well, A.A.; Mutka, H.; Mulder, F.M. Multiple Li positions inside oxygen octahedra in lithiated TiO_2 anatase. *J. Am. Chem. Soc.* **2003**, *125*, 840–848. [CrossRef] [PubMed]
25. Mancini, M.; Nobili, F.; Tossici, R.; Wohlfahrt-Mehrens, M.; Marassi, R. High performance, environmentally friendly and low cost anodes for lithium-ion battery based on TiO_2 anatase and water soluble binder carboxymethyl cellulose. *J. Power Sources* **2011**, *196*, 9665–9671. [CrossRef]
26. Xie, M.; Sun, X.; Zhou, C.; Cavanagh, A.S.; Sun, H.; Hu, T.; Wang, G.; Lian, J.; George, S.M. Amorphous Ultrathin TiO_2 atomic layer deposition films on carbon nanotubes as anodes for lithium ion batteries. *J. Electrochem. Soc.* **2015**, *162*, A974–A981. [CrossRef]
27. Jiang, C.; Zhang, J. Nanoengineering titania for high rate lithium storage: A review. *J. Mater. Sci. Technol.* **2013**, *29*, 97–122. [CrossRef]
28. Nuspl, G.; Yoshizawa, K.; Yamabe, T. Lithium intercalation in TiO_2 modifications. *J. Mater. Chem.* **1997**, *7*, 2529–2536. [CrossRef]
29. Van de Krol, R.; Goossens, A.; Schoonman, J. Spatial extent of lithium intercalation in anatase TiO_2. *J. Phys. Chem. B* **1999**, *103*, 7151–7159. [CrossRef]
30. Koudriachova, M.V.; Harrison, N.M.; De Leeuw, S.W. Diffusion of Li-ions in rutile. An ab initio study. *Solid State Ion.* **2003**, *157*, 35–38. [CrossRef]
31. Lindström, H.; Södergren, S.; Solbrand, A.; Rensmo, H.; Hjelm, J.; Hagfeldt, A.; Lindquist, S.-E. Li^+ ion insertion in TiO_2 (anatase). 2. Voltammetry on nanoporous films. *J. Phys. Chem. B* **1997**, *101*, 7717–7722. [CrossRef]

32. Zhang, Y.; Tang, Y.; Li, W.; Chen, X. Nanostructured TiO_2-based anode materials for high-performance rechargeable lithium-ion batteries. *ChemNanoMat* **2016**, *2*, 764–775. [CrossRef]
33. Liu, Z.; Andreev, Y.G.; Armstrong, A.R.; Brutti, S.; Ren, Y.; Bruce, P.G. Nanostructured TiO_2(B): The effect of size and shape on anode properties for Li-ionbatteries. *Prog. Nat. Sci. Mater. Int.* **2013**, *23*, 235–244. [CrossRef]
34. Whittingham, M.S. Lithium batteries and cathode materials. *Chem. Rev.* **2004**, *104*, 4271–4301. [CrossRef] [PubMed]
35. Fergus, J.W. Recent developments in cathode materials for lithium ion batteries. *J. Power Sources* **2010**, *195*, 939–954. [CrossRef]
36. Xu, Z.R.; Gao, L.B.; Liu, Y.J.; Li, L. Recent developments in the doped $LiFePO_4$ cathode materials for power lithium ion batteries. *J. Electrochem. Soc.* **2016**, *163*, A2600–A2610. [CrossRef]
37. Qi, Z.; Koenig, G.M., Jr. High-performance $LiCoO_2$ sub-micrometer materials from scalable microparticle template processing. *Chem. Sel.* **2016**, *1*, 3992–3999. [CrossRef]
38. Eftekhari, A. $LiFePO_4$/C nanocomposites for lithium-ion batteries. *J. Power Sources* **2017**, *343*, 395–411. [CrossRef]
39. Scrosati, B. Lithium rocking chair batteries: An old concept? *J. Electrochem. Soc.* **1992**, *139*, 2776–2781. [CrossRef]
40. Moseley, P.T.; Garche, J. *Electrochemical Energy Storage For Renewable Sources and Grid Balancing*, 1st ed.; Elsevier: Amsterdam, The Netherlands, 2014; ISBN 9780444626165.
41. Yang, P. *The Chemistry of Nanostructured Materials*; World Scientific Publishing Co.: Singapore, 2011; ISBN 9814313068.
42. Wang, Y.; Liu, B.; Li, Q.; Cartmell, S.; Ferrara, S.; Deng, Z.D.; Xiao, J. Lithium and lithium ion batteries for applications in microelectronic devices: A review. *J. Power Sources* **2015**, *286*, 330–345. [CrossRef]
43. Abraham, K.M. Prospects and limits of energy storage in batteries. *J. Phys. Chem. Lett.* **2015**, *6*, 830–844. [CrossRef] [PubMed]
44. Kavan, L.; Grätzel, M.; Gilbert, S.E.; Klemenz, C.; Scheel, H.J. Electrochemical and photoelectrochemical investigation of single crystal anatase. *J. Am. Chem. Soc.* **1996**, *118*, 6716–6723. [CrossRef]
45. Simons, D.; Roy, R. Pressure-temperature studies of anatase, brookite, rutile, and TiO_2(II). *Am. Mineral.* **1968**, *53*, 1929–1939. [CrossRef]
46. Yin, Z.F.; Wu, L.; Yang, H.G.; Su, Y.H. Recent progress in biomedical applications of titanium dioxide. *Phys. Chem. Chem. Phys.* **2013**, *15*, 4844–4858. [CrossRef] [PubMed]
47. Shannon, R.D.; Pask, J.A. Kinetics of the anatase-rutile transformation. *J. Am. Ceram. Soc.* **1965**, *48*, 391–398. [CrossRef]
48. Koudriachova, M.; Harrison, N.; de Leeuw, S. Effect of diffusion on lithium intercalation in titanium dioxide. *Phys. Rev. Lett.* **2001**, *86*, 1275–1278. [CrossRef] [PubMed]
49. Zhang, Y.; Jiang, Z.; Huang, J.; Lim, Y.W.L.; Li, W.; Deng, J.; Gong, D.; Tang, Y.; Lai, Y.; Chen, Z. Titanate and titania nanostructured materials for environmental and energy applications: A review. *RSC Adv.* **2015**, *5*, 79479–79510. [CrossRef]
50. Yan, X.; Wang, Z.; He, M.; Hou, Z.; Xia, T.; Liu, G.; Chen, X. TiO_2 Nanomaterials as Anode Materials for Lithium-Ion Rechargeable Batteries. *Energy Technol.* **2015**, *3*, 801–814. [CrossRef]
51. Wagemaker, M.; van de Krol, R.; Kentgens, A.P.M.; van Well, A.A.; Mulder, F.M. Two phase morphology limits lithium diffusion in TiO_2 (anatase): A ^{7}Li MAS NMR study. *J. Am. Chem. Soc.* **2001**, *123*, 11454–11461. [CrossRef] [PubMed]
52. Vittadini, A.; Casarin, M.; Selloni, A. Structure and stability of TiO_2-B surfaces: A density functional study. *J. Phys. Chem. C* **2009**, *113*, 18973–18977. [CrossRef]
53. Cromer, D.T.; Herrington, K. The structures of anatase and rutile. *J. Am. Chem. Soc.* **1955**, *77*, 4708–4709. [CrossRef]
54. Yang, Z.; Choi, D.; Kerisit, S.; Rosso, K.M.; Wang, D.; Zhang, J.; Graff, G.; Liu, J. Nanostructures and lithium electrochemical reactivity of lithium titanites and titanium oxides: A review. *J. Power Sources* **2009**, *192*, 588–598. [CrossRef]
55. Zukalova, M.; Kalbac, M.; Kavan, L.; Zukalová, M.; Kalbáč, M.; Exnar, I.; Graetzel, M. Pseudocapacitive lithium storage in TiO_2 (B). *Chem. Mater.* **2005**, *17*, 1248–1255. [CrossRef]

56. Su, X.; Wu, Q.; Zhan, X.; Wu, J.; Wei, S.; Guo, Z. Advanced titania nanostructures and composites for lithium ion battery. *J. Mater. Sci.* **2011**, *47*, 2519–2534. [CrossRef]
57. Wagemaker, M.; Borghols, W.J.H.; Mulder, F.M. Large impact of particle size on insertion reactions. A case for anatase Li_xTiO_2. *J. Am. Chem. Soc.* **2007**, *129*, 4323–4327. [CrossRef] [PubMed]
58. Jiang, C.; Wei, M.; Qi, Z.; Kudo, T.; Honma, I.; Zhou, H. Particle size dependence of the lithium storage capability and high rate performance of nanocrystalline anatase TiO_2 electrode. *J. Power Sources* **2007**, *166*, 239–243. [CrossRef]
59. Wagemaker, M.; Borghols, W.J.H.; van Eck, E.R.H.; Kentgens, A.P.M.; Kearley, G.J.; Mulder, F.M. The Influence of size on phase morphology and Li-ion mobility in nanosized lithiated anatase TiO_2. *Chem. Eur. J.* **2007**, *13*, 2023–2028. [CrossRef] [PubMed]
60. Sudant, G.; Baudrin, E.; Larcher, D.; Tarascon, J.M. Electrochemical lithium reactivity with nanotextured anatase-type TiO_2. *J. Mater. Chem.* **2005**, *15*, 1263–1269. [CrossRef]
61. Hu, Y.S.; Kienle, L.; Guo, Y.G.; Maier, J. High lithium electroactivity of nanometer-sized rutile TiO_2. *Adv. Mater.* **2006**, *18*, 1421–1426. [CrossRef]
62. Kavan, L.; Kalbac, M.; Zukalova, M.; Exnar, I.; Lorenzen, V.; Nesper, R.; Graetzel, M. Lithium storage in nanostructured TiO_2 made by hydrothermal growth. *Chem. Mater.* **2004**, *16*, 477–485. [CrossRef]
63. Borghols, W.J.H.; Wagemaker, M.; Lafont, U.; Kelder, E.M.; Mulder, F.M. Impact of nanosizing on lithiated rutile TiO_2. *Chem. Mater.* **2008**, *20*, 2949–2955. [CrossRef]
64. Jamnik, J.; Maier, J. Nanocrystallinity effects in lithium battery materials. *Phys. Chem. Chem. Phys.* **2003**, *5*, 5215–5220. [CrossRef]
65. Jiang, C.; Honma, I.; Kudo, T.; Zhou, H. Nanocrystalline rutile TiO_2 electrode for high-capacity and high-rate lithium storage. *Electrochem. Solid State Lett.* **2007**, *10*, A127–A129. [CrossRef]
66. Sushko, M.L.; Rosso, K.M.; Liu, J. Size effects on Li^+/electron conductivity in TiO_2 nanoparticles. *J. Phys. Chem. Lett.* **2010**, *1*, 1967–1972. [CrossRef]
67. Kubiak, P.; Fröschl, T.; Hüsing, N.; Hörmann, U.; Kaiser, U.; Schiller, R.; Weiss, C.K.; Landfester, K.; Wohlfahrt-Mehrens, M. TiO_2 anatase nanoparticle networks: Synthesis, structure, and electrochemical performance. *Small* **2011**, *7*, 1690–1696. [CrossRef] [PubMed]
68. Wilhelm, O.; Pratsinis, S.E.; de Chambrier, E.; Crouzet, M.; Exnar, I. Electrochemical performance of granulated titania nanoparticles. *J. Power Sources* **2004**, *134*, 197–201. [CrossRef]
69. Liang, J.; Wang, Z.; Li, Z.; Wang, X.; Yu, K. Fabrication of nanostructured TiO_2 using a solvothermal reaction for lithium-ion batteries. *Nanomater. Nanotechnol.* **2016**, *6*, 15. [CrossRef]
70. Kang, J.; Kim, D.H.; Mathew, V.; Lim, J.S.; Gim, J.; Kim, J. Particle size effect of anatase TiO_2 nanocrystals for lithium-ion batteries. *J. Electrochem. Soc.* **2011**, *158*, A59–A62. [CrossRef]
71. Liu, L.; Fan, Q.; Sun, C.; Gu, X.; Li, H.; Gao, F.; Chen, Y.; Dong, L. Synthesis of sandwich-like TiO_2@C composite hollow spheres with high rate capability and stability for lithium-ion batteries. *J. Power Sources* **2013**, *221*, 141–148. [CrossRef]
72. Zhang, L.; Wang, Y.; Jiu, H.; Qiu, H.; Wang, H. Porous TiO_2/C nanocomposite shells as a high-performance anode material for lithium-ion batteries. *ACS Appl. Mater. Interface* **2013**, *5*, 6478–6483. [CrossRef]
73. Wang, D.; Choi, D.; Li, J.; Yang, Z.; Nie, Z.; Kou, R.; Hu, D.; Wang, C.; Saraf, L.V.; Zhang, J.; et al. Self-assembled TiO_2—Graphene hybrid insertion. *ACS Nano* **2009**, *3*, 907–914. [CrossRef] [PubMed]
74. Cao, F.F.; Guo, Y.G.; Zheng, S.F.; Wu, X.L.; Jiang, L.Y.; Bi, R.R.; Wan, L.J.; Maier, J. Symbiotic coaxial nanocables: Facile synthesis and an efficient and elegant morphological solution to the lithium storage problem. *Chem. Mater.* **2010**, *22*, 1908–1914. [CrossRef]
75. Tao, H.C.; Fan, L.Z.; Yan, X.; Qu, X. In situ synthesis of TiO_2-graphene nanosheets composites as anode materials for high-power lithium ion batteries. *Electrochim. Acta* **2012**, *69*, 328–333. [CrossRef]
76. Winsberg, J.; Hagemann, T.; Janoschka, T.; Hager, M.D.; Schubert, U.S. Redox-flow batteries: From metals to organic redox-active materials. *Angew. Chem. Int. Ed.* **2017**, *56*, 686–711. [CrossRef] [PubMed]
77. Qi, Z.; Koenig, G.M. Flow battery systems with solid electroactive materials. *J. Vac. Sci. Technol. B* **2017**, *35*, 040801. [CrossRef]
78. Pan, F.; Wang, Q. Redox species of redox flow batteries: A review. *Molecules* **2015**, *20*, 20499–20517. [CrossRef] [PubMed]

79. Wang, Q.; Zakeeruddin, S.M.; Wang, D.; Exnar, I.; Grätzel, M. Redox targeting of insulating electrode materials: A new approach to high-energy-density batteries. *Angew. Chem. Int. Ed.* **2006**, *45*, 8197–8200. [CrossRef] [PubMed]
80. Skyllas-Kazacos, M.; Grossmith, F. Efficient vanadium redox flow cell. *J. Electrochem. Soc.* **1987**, *134*, 2950–2953. [CrossRef]
81. Duduta, M.; Ho, B.; Wood, V.C.; Limthongkul, P.; Brunini, V.E.; Carter, W.C.; Chiang, Y.-M. Semi-solid lithium rechargeable flow battery. *Adv. Energy Mater.* **2011**, *1*, 511–516. [CrossRef]
82. Huang, Q.; Li, H.; Grätzel, M.; Wang, Q. Reversible chemical delithiation/lithiation of $LiFePO_4$: Towards a redox flow lithium-ion battery. *Phys. Chem. Chem. Phys.* **2013**, *15*, 793–1797. [CrossRef] [PubMed]
83. Pan, F.; Yang, J.; Huang, Q.; Wang, X.; Huang, H.; Wang, Q. Redox targeting of anatase TiO_2 for redox flow lithium-ion batteries. *Adv. Energy Mater.* **2014**, *4*, 1400567. [CrossRef]
84. Jia, C.; Pan, F.; Zhu, Y.G.; Huang, Q.; Lu, L.; Wang, Q. High–energy density nonaqueous all redox flow lithium battery enabled with apolymeric membrane. *Sci. Adv.* **2015**, *1*, e1500886. [CrossRef] [PubMed]
85. Wang, D.; Choi, D.; Yang, Z.; Viswanathan, V.V.; Nie, Z.; Wang, C.; Song, Y.; Zhang, J.-G.; Liu, J. Synthesis and Li-ion insertion properties of highly crystalline mesoporous rutile TiO_2. *Chem. Mater.* **2008**, *20*, 3435–3442. [CrossRef]
86. Qiao, H.; Tao, D.; Wang, Y.; Cai, Y.; Huang, F.; Yang, X.; Wei, J.; Wei, Q. Electrochemical charge storage of flowerlike rutile TiO_2 nanorods. *Chem. Phys. Lett.* **2010**, *490*, 180–183. [CrossRef]
87. Lan, Y.; Gao, X.; Zhu, H.; Zheng, Z.; Yan, T.; Wu, F.; Ringer, S.P.; Song, D. Titanate nanotubes and nanorods prepared from rutile powder. *Adv. Funct. Mater.* **2005**, *15*, 1310–1318. [CrossRef]
88. Kim, J.; Cho, J. Rate Characteristics of anatase TiO_2 nanotubes and nanorods for lithium battery anode materials at room temperature. *J. Electrochem. Soc.* **2007**, *154*, A542–A546. [CrossRef]
89. Bao, S.J.; Bao, Q.L.; Li, C.M.; Dong, Z.L. Novel porous anatase TiO_2 nanorods and their high lithium electroactivity. *Electrochem. Commun.* **2007**, *9*, 1233–1238. [CrossRef]
90. Gao, X.; Zhu, H.; Pan, G.; Ye, S.; Lan, Y.; Wu, F.; Song, D. Preparation and electrochemical characterization of anatase nanorods for lithium-inserting electrode material. *J. Phys. Chem. B* **2004**, *108*, 2868–2872. [CrossRef]
91. Khomane, R.B. Microemulsion-mediated sol-gel synthesis of mesoporous rutile TiO_2 nanoneedles and its performance as anode material for Li-ion batteries. *J. Colloid Interface Sci.* **2011**, *356*, 369–372. [CrossRef] [PubMed]
92. Wang, Y.; Wu, M.; Zhang, W.F. Preparation and electrochemical characterization of TiO_2 nanowires as an electrode material for lithium-ion batteries. *Electrochim. Acta* **2008**, *53*, 7863–7868. [CrossRef]
93. Wu, F.; Li, X.; Wang, Z.; Guo, H.; Wu, L.; Xiong, X.; Wang, X. A novel method to synthesize anatase TiO_2 nanowires as an anode material for lithium-ion batteries. *J. Alloy. Compd.* **2011**, *509*, 3711–3715. [CrossRef]
94. Armstrong, A.R.; Armstrong, G.; Canales, J.; Bruce, P.G. TiO_2-B nanowires. *Angew. Chem. Int. Ed.* **2004**, *116*, 2286–2288. [CrossRef] [PubMed]
95. Tammawat, P.; Meethong, N. Synthesis and characterization of stable and binder-free electrodes of TiO_2 nanofibers for Li-ion batteries. *J. Nanomater.* **2013**, *2013*, 413692. [CrossRef]
96. Goriparti, S.; Miele, E.; Prato, M.; Scarpellini, A.; Marras, S.; Monaco, S.; Toma, A.; Messina, G.C.; Alabastri, A.; de Angelis, F.; et al. Direct Synthesis of carbon-doped TiO_2-bronze nanowires as anode materials for high performance lithium-ion batteries. *ACS Appl. Mater. Interfaces* **2015**, *7*, 25139–25146. [CrossRef] [PubMed]
97. Shen, L.; Zhang, X.; Li, H.; Yuan, C.; Cao, G. Design and tailoring of a three-dimensional TiO_2-graphene-carbon nanotube nanocomposite for fast lithium storage. *J. Phys. Chem. Lett.* **2011**, *2*, 3096–3101. [CrossRef]
98. Wang, J.; Zhou, Y.; Xiong, B.; Zhao, Y.; Huang, X.; Shao, Z. Fast lithium-ion insertion of TiO_2 nanotube and graphene composites. *Electrochim. Acta* **2013**, *88*, 847–857. [CrossRef]
99. He, L.; Ma, R.; Du, N.; Ren, J.; Wong, T.; Li, Y.; Lee, S.T. Growth of TiO_2 nanorod arrays on reduced graphene oxide with enhanced lithium-ion storage. *J. Mater. Chem.* **2012**, *22*, 19061–19066. [CrossRef]
100. Zuniga, L.; Agubra, V.; Flores, D.; Campos, H.; Villareal, J.; Alcoutlabi, M. Multichannel hollow structure for improved electrochemical performance of TiO_2/Carbon composite nanofibers as anodes for lithium ion batteries. *J. Alloy. Compd.* **2016**, *686*, 733–743. [CrossRef]
101. Thirugunanama, L.; Kaveric, S.; Etacherib, V.; Ramaprabhua, S.; Duttad, M.; Polb, V.G. Electrospun nanoporous TiO_2 nanofibers wrapped with reduced graphene oxide for enhanced and rapid lithium-ion storage. *Mater. Charact.* **2017**, *131*, 64–71. [CrossRef]

102. Ding, S.; Chen, J.S.; Luan, D.; Yin, F.; Boey, C.; Madhavib, S.; Lou, X.W.D. Graphene-supported anatase TiO_2 nanosheets for fast lithium storage. *Chem. Commun.* **2011**, *47*, 5780–5782. [CrossRef] [PubMed]
103. Xin, X.; Zhou, X.; Wu, J.; Yao, X.; Liu, Z. Scalable synthesis of TiO_2/graphene nanostructured composite with high-rate performance for lithium ion batteries. *ACS Nano* **2012**, *6*, 11035–11043. [CrossRef] [PubMed]
104. Choi, D.; Wang, D.; Viswanathan, V.V.; Bae, I.; Wang, W.; Nie, Z.; Zhang, J.; Graff, G.L.; Liu, J.; Yang, Z.; et al. Li-ion batteries from $LiFePO_4$ cathode and anatase/graphene composite anode for stationary energy storage. *Electrochem. Commun.* **2010**, *12*, 378–381. [CrossRef]
105. Wang, H.E.; Cheng, H.; Liu, C.; Chen, X.; Jiang, Q.; Lu, Z.; Li, Y.Y.; Chung, C.Y.; Zhang, W.; Zapien, J.A.; et al. Facile synthesis and electrochemical characterization of porous and dense TiO_2 nanospheres for lithium-ion battery applications. *J. Power Sources* **2011**, *196*, 6394–6399. [CrossRef]
106. Xiao, L.; Cao, M.; Mei, D.; Guo, Y.; Yao, L.; Qu, D.; Deng, B. Preparation and electrochemical lithium storage features of TiO_2 hollow spheres. *J. Power Sources* **2013**, *238*, 197–202. [CrossRef]
107. Saravanan, K.; Ananthanarayanan, K.; Balaya, P. Mesoporous TiO_2 with high packing density for superior lithium storage. *Energy Environ. Sci.* **2010**, *3*, 939–948. [CrossRef]
108. Wang, H.E.; Jin, J.; Cai, Y.; Xu, J.M.; Chen, D.S.; Zheng, X.F.; Deng, Z.; Li, Y.; Bello, I.; Su, B.L. Facile and fast synthesis of porous TiO_2 spheres for use in lithium ion batteries. *J. Colloid Interface Sci.* **2014**, *417*, 144–151. [CrossRef] [PubMed]
109. Zhang, Z.H.; Zhang, L.D.; Li, W.; Yu, A.S.; Wu, P.Y. Carbon-coated mesoporous TiO_2 nanocrystals grown on graphene for lithium-ion batteries. *ACS Appl. Mater. Interfaces* **2015**, *7*, 10395–10400. [CrossRef] [PubMed]
110. Jiang, Y.M.; Wang, K.X.; Guo, X.X.; Wei, X.; Wang, J.F.; Chen, J.S. Mesoporous titania rods as an anode material for high performance lithium-ion batteries. *J. Power Sources* **2012**, *214*, 298–302. [CrossRef]
111. Bresser, D.; Paillard, E.; Binetti, E.; Krueger, S.; Striccoli, M.; Winter, M.; Passerini, S. Percolating networks of TiO_2 nanorods and carbon for high power lithium insertion electrodes. *J. Power Sources* **2012**, *206*, 301–309. [CrossRef]
112. Zhang, X.; Chen, H.; Xie, Y.; Guo, J. Ultralong life lithium-ion battery anode with superior high-rate capability and excellent cyclic stability from mesoporous $Fe2O_3$@TiO_2 core–shell nanorods. *J. Mater. Chem. A* **2014**, *2*, 3912–3918. [CrossRef]
113. Wang, H.-G.; Li, Y.-H.; Liu, W.-Q.; Wan, Y.-C.; Li, Y.-W.; Duan, Q. One-step facile synthesis of TiO_2/Fe_2O_3 fiber-in-tube hierarchical heterostructures with improved lithium-ion battery performance. *RSC Adv.* **2014**, *4*, 23125–23130. [CrossRef]
114. Cai, Y.; Wang, H.E.; Huang, S.Z.; Yuen, M.F.; Cai, H.H.; Wang, C.; Yu, Y.; Li, Y.; Zhang, W.J.; Su, B.L. Porous TiO_2 urchins for high performance Li-ion battery electrode: Facile synthesis, characterization and structural evolution. *Electrochim. Acta* **2016**, *210*, 206–214. [CrossRef]
115. Wang, X.; Jia, Z.; Liu, F.; Liang, H.; You, X.; Wang, K.; Lou, X.; Shuang, W.; Xiao, L.; Cai, B.; et al. The template-free synthesis of hierarchically porous anatase TiO_2 via acid-etching for enhancing the cycling stability and reversible capacity of lithium ion batteries. *RSC Adv.* **2016**, *6*, 48985–48994. [CrossRef]
116. Maier, J. Mass storage in space charge regions of nano-sized systems, Nano-ionics. Part V. *Faraday Discuss. Chem. Soc.* **2007**, *134*, 51–66. [CrossRef]
117. Shin, J.-Y.; Samuelis, D.; Maier, J. Sustained lithium-storage performance of hierarchical, nanoporous anatase TiO_2 at high rates: Emphasis on interfacial storage phenomena. *Adv. Funct. Mater.* **2011**, *21*, 3464–3472. [CrossRef]
118. Jin, J.; Huang, S.Z.; Li, Y.; Tian, H.; Wang, H.E.; Yu, Y.; Chen, L.H.; Hasan, T.; Su, B.L. Hierarchical nanosheet-constructed yolk-shell TiO_2 porous microspheres for lithium batteries with high capacity, superior rate and long cycle capability. *Nanoscale* **2015**, *7*, 12979–12989. [CrossRef] [PubMed]
119. Lui, G.; Li, G.; Wang, X.; Jiang, G.; Lin, E.; Fowler, M.; Yu, A.; Chen, Z. Flexible, three-dimensional ordered macroporous TiO_2 electrode with enhanced electrode-electrolyte interaction in high-power li-ion batteries. *Nano Energy* **2016**, *24*, 72–77. [CrossRef]
120. Ye, J.; Baumgaertel, A.C.; Wang, Y.M.; Biener, J.; Biener, M.M. Structural optimization of 3D porous electrodes for high-rate performance lithium ion batteries. *Nano Lett.* **2015**, *9*, 2194–2202. [CrossRef] [PubMed]
121. Ge, M.; Cao, C.; Huang, J.; Li, S.; Chen, Z.; Zhang, K.Q.; Aldeyab, S.S.; Lai, Y. A review of one-dimensional TiO_2 nanostructured materials for environmental and energy applications. *J. Mater. Chem. A* **2016**, *4*, 6772–6801. [CrossRef]

122. Zwilling, V.; Aucouturier, M.; Darque-Ceretti, E. Anodic oxidation of titanium and TA6V alloy in chromic media. An electrochemical approach. *Electrochim. Acta* **1999**, *45*, 921–929. [CrossRef]
123. Kelly, J.J. The influence of fluoride ions on the passive dissolution of titanium. *Electrochim. Acta* **1979**, *24*, 1273–1282. [CrossRef]
124. Gong, D.; Grimes, C.A.; Varghese, O.K.; Hu, W.; Singh, R.S.; Chen, Z.; Dickey, E.C. Titanium oxide nanotube arrays prepared by anodic oxidation. *J. Mater. Res.* **2001**, *16*, 3331–3334. [CrossRef]
125. Madian, M.; Giebeler, L.; Klose, M.; Jaumann, T.; Uhlemann, M.; Gebert, A.; Oswald, S.; Ismail, N.; Eychmüller, A.; Eckert, J. Self-Organized TiO_2/CoO Nanotubes as Potential Anode Materials for Lithium Ion Batteries. *ACS Sustain. Chem. Eng.* **2015**, *3*, 909–919. [CrossRef]
126. Mor, G.K.; Varghese, O.K.; Paulose, M.; Mukherjee, N.; Grimes, C.A. Fabrication of tapered, conical-shaped titania nanotubes. *J. Mater. Res.* **2003**, *18*, 2588–2593. [CrossRef]
127. Ruan, C.; Paulose, M.; Varghese, O.K.; Mor, G.K.; Grimes, C.A. Fabrication of highly ordered TiO_2 nanotube arrays using an organic electrolyte. *J. Phys. Chem. B* **2005**, *109*, 15754–15759. [CrossRef] [PubMed]
128. Albu, S.P.; Ghicov, A.; Macak, J.M.; Schmuki, P. 250 μm long anodic TiO_2 nanotubes with hexagonal self-ordering. *Phys. Status Solidi Rapid Res. Lett.* **2007**, *1*, R65–R67. [CrossRef]
129. Quan, X.; Yang, S.; Ruan, X.; Zhao, H. Preparation of titania nanotubes and their environmental applications as electrode. *Environ. Sci. Technol.* **2005**, *39*, 3770–3775. [CrossRef] [PubMed]
130. Macak, J.M.; Tsuchiya, H.; Taveira, L.; Aldabergerova, S.; Schmuki, P. Smooth anodic TiO_2 nanotubes. *Angew. Chem. Int. Ed.* **2005**, *44*, 7463–7465. [CrossRef] [PubMed]
131. Macak, J.M.; Sirotna, K.; Schmuki, P. Self-organized porous titanium oxide prepared in Na_2SO_4/NaF electrolytes. *Electrochim. Acta* **2005**, *50*, 3679–3684. [CrossRef]
132. Tsuchiya, H.; Macak, J.M.; Taveira, L.; Balaur, E.; Ghicov, A.; Sirotna, K.; Schmuki, P. Self-organized TiO_2 nanotubes prepared in ammonium fluoride containing acetic acid electrolytes. *Electrochem. Commun.* **2005**, *7*, 576–580. [CrossRef]
133. Jessensky, O.; Müller, F.; Gösele, U. Self-organized formation of hexagonal pore arrays in anodic alumina. *Appl. Phys. Lett.* **1998**, *72*, 1173–1175. [CrossRef]
134. Beranek, R.; Hildebrand, H.; Schmuki, P. Self-organized porous titanium oxide prepared in H_2SO_4/HF electrolytes. *Electrochem. Solid State Lett.* **2003**, *6*, B12–B14. [CrossRef]
135. Grimes, C.A. Synthesis and application of highly ordered arrays of TiO_2 nanotubes. *J. Mater. Chem.* **2007**, *17*, 1451. [CrossRef]
136. Parkhutik, V.P.; Shershulsky, V.I. Theoretical modelling of porous oxide growth on aluminium. *J. Phys. D Appl. Phys.* **1992**, *25*, 1258–1263. [CrossRef]
137. Macdonald, D.D. On the formation of voids in anodic oxide films on aluminum. *J. Electrochem. Soc.* **1993**, *140*, L27–L30. [CrossRef]
138. Jaroenworaluck, A.; Regonini, D.; Bowen, C.R.; Stevens, R.; Allsopp, D. Macro, micro and nanostructure of TiO_2 anodised films prepared in a fluorine-containing electrolyte. *J. Mater. Sci.* **2007**, *42*, 6729–6734. [CrossRef]
139. Siejka, J. An O^{18} study of field-assisted pore formation in compact anodic oxide films on aluminum. *J. Electrochem. Soc.* **1977**, *124*, 883–891. [CrossRef]
140. Lohrengel, M.M. Thin anodic oxide layers on aluminium and other valve metals: High field regime. *Mater. Sci. Eng. Rep.* **1993**, *11*, 243–294. [CrossRef]
141. Thompson, G.E. Porous anodic alumina: Fabrication, characterization and applications. *Thin Solid Films* **1997**, *297*, 192–201. [CrossRef]
142. Kirchgeorg, R.; Kallert, M.; Liu, N.; Hahn, R.; Killian, M.S.; Schmuki, P. Key factors for an improved lithium ion storage capacity of anodic TiO_2 nanotubes. *Electrochim. Acta* **2016**, *198*, 56–65. [CrossRef]
143. Han, H.; Song, T.; Lee, E.K.; Devadoss, A.; Jeon, Y.; Ha, J.; Chung, Y.C.; Choi, Y.M.; Jung, Y.G.; Paik, U. Dominant factors governing the rate capability of a TiO_2 nanotube anode for high power lithium ion batteries. *ACS Nano* **2012**, *6*, 8308–8315. [CrossRef] [PubMed]
144. Wei, Z.; Liu, Z.; Jiang, R.; Bian, C.; Huang, T.; Yu, A. TiO_2 nanotube array film prepared by anodization as anode material for lithium ion batteries. *J. Solid State Electrochem.* **2009**, *14*, 1045–1050. [CrossRef]
145. Shannon, R.D. Phase transformation studies in TiO_2 supporting different defect mechanisms in vacuum-reduced and hydrogen-reduced rutile. *J. Appl. Phys.* **1964**, *35*, 3414–3416. [CrossRef]

146. Roman, I.; Trusca, R.D.; Soare, M.L.; Fratila, C.; Krasicka-Cydzik, E.; Stan, M.S.; Dinischiotu, A. Titanium dioxide nanotube films: Preparation, characterization and electrochemical biosensitivity towards alkaline phosphatase. *Mater. Sci. Eng. C* **2014**, *37*, 374–382. [CrossRef] [PubMed]
147. Mor, G.K.; Prakasam, H.E.; Varghese, O.K.; Shankar, K.; Grimes, C.A. Vertically oriented Ti-Fe-O nanotube array films: Toward a useful material architecture for solar spectrum water photoelectrolysis. *Nano Lett.* **2007**, *7*, 2356–2364. [CrossRef] [PubMed]
148. Ivanov, S.; Cheng, L.; Wulfmeier, H.; Albrecht, D.; Fritze, H.; Bund, A. Electrochemical behavior of anodically obtained titania nanotubes in organic carbonate and ionic liquid based Li ion containing electrolytes. *Electrochim. Acta* **2013**, *104*, 228–235. [CrossRef]
149. Li, H.; Martha, S.K.; Unocic, R.R.; Luo, H.; Dai, S.; Qu, J. High cyclability of ionic liquid-produced TiO_2 nanotube arrays as an anode material for lithium-ion batteries. *J. Power Sources* **2012**, *218*, 88–92. [CrossRef]
150. Ryu, W.H.; Nam, D.H.; Ko, Y.S.; Kim, R.H.; Kwon, H.-S. Electrochemical performance of a smooth and highly ordered TiO_2 nanotube electrode for Li-ion batteries. *Electrochim. Acta* **2012**, *61*, 19–24. [CrossRef]
151. Fang, H.T.; Liu, M.; Wang, D.W.; Sun, T.; Guan, D.S.; Li, F.; Zhou, J.; Sham, T.K.; Cheng, H.M. Comparison of the rate capability of nanostructured amorphous and anatase TiO_2 for lithium insertion using anodic TiO_2 nanotube arrays. *Nanotechnology* **2009**, *20*, 225701. [CrossRef] [PubMed]
152. Tighineanu, A.; Ruff, T.; Albu, S.; Hahn, R.; Schmuki, P. Conductivity of TiO_2 nanotubes: Influence of annealing time and temperature. *Chem. Phys. Lett.* **2010**, *494*, 260–263. [CrossRef]
153. Guan, D.; Cai, C.; Wang, Y. Amorphous and Crystalline TiO_2 Nanotube Arrays for Enhanced Li-ion intercalation properties. *J. Nanosci. Nanotechnol.* **2011**, *11*, 3641–3650. [CrossRef] [PubMed]
154. Wang, Y.; Liu, S.; Huang, K.; Fang, D.; Zhuang, S. Electrochemical properties of freestanding TiO_2 nanotube membranes annealed in Ar for lithium anode material. *J. Solid State Electrochem.* **2012**, *16*, 723–729. [CrossRef]
155. Liu, D.; Xiao, P.; Zhang, Y.; Garcia, B.B.; Zhang, Q.; Guo, Q.; Champion, R.; Cao, G. TiO_2 nanotube arrays annealed in N_2 for efficient lithium-ion intercalation. *J. Phys. Chem. C* **2008**, *112*, 11175–11180. [CrossRef]
156. Lu, Z.; Yip, C.T.; Wang, L.; Huang, H.; Zhou, L. Hydrogenated TiO_2 nanotube arrays as high-rate anodes for lithium-ion microbatteries. *ChemPlusChem* **2012**, *77*, 991–1000. [CrossRef]
157. Wei, W.; Oltean, G.; Tai, C.W.; Edström, K.; Björefors, F.; Nyholm, L. High energy and power density TiO_2 nanotube electrodes for 3D Li-ion microbatteries. *J. Mater. Chem. A* **2013**, *1*, 8160–8169. [CrossRef]
158. Liu, G.; Hoivik, N.; Wang, K. Small diameter TiO_2 nanotubes with enhanced photoresponsivity. *Electrochem. Commun.* **2013**, *28*, 107–110. [CrossRef]
159. Kilinç, N.; Şennik, E.; Işik, M.; Ahsen, A.Ş.; Öztürk, O.; Öztürk, Z.Z. Fabrication and gas sensing properties of C-doped and un-doped TiO_2 nanotubes. *Ceram. Int.* **2014**, *40*, 109–115. [CrossRef]
160. Mole, F.; Wang, J.; Clayton, D.A.; Xu, C.; Pan, S. Highly conductive nanostructured C-TiO_2 electrodes with enhanced electrochemical stability and double layer charge storage capacitance. *Langmuir* **2012**, *28*, 10610–10619. [CrossRef] [PubMed]
161. Chen, Y.; Tang, Y.; Luo, S.; Liu, C.; Li, Y. TiO_2 nanotube arrays co-loaded with Au nanoparticles and reduced graphene oxide: Facile synthesis and promising photocatalytic application. *J. Alloy. Compd.* **2013**, *578*, 242–248. [CrossRef]
162. Madian, M.; Ummethala, R.; Naga, A.O.A.E.; Ismail, N.; Rümmeli, M.H.; Eychmüller, A.; Giebeler, L. Ternary CNTs@TiO_2/CoO nanotube composites: Improved anode materials for high performance lithium ion batteries. *Materials* **2017**, *10*, 678. [CrossRef] [PubMed]
163. Fan, Y.; Zhang, N.; Zhang, L.; Shao, H.; Wang, J.; Zhang, J.; Cao, C. Co_3O_4-coated TiO_2 nanotube composites synthesized through photo-deposition strategy with enhanced performance for lithium-ion batteries. *Electrochim. Acta* **2013**, *94*, 285–293. [CrossRef]
164. Cao, C.L.; Hu, C.G.; Shen, W.D.; Wang, S.X.; Liu, H.; Wang, J.L. Cobalt oxide modified highly ordered TiO_2 nanotube arrays: Enhanced visible light photoelectrochemical properties. *Sci. Adv. Mater.* **2013**, *5*, 1256–1263. [CrossRef]
165. Macak, J.M.; Gong, B.G.; Hueppe, M.; Schmuki, P. Filling of TiO_2 nanotubes by self-doping and electrodeposition. *Adv. Mater.* **2007**, *19*, 3027–3031. [CrossRef]
166. Mohapatra, S.K.; Banerjee, S.; Misra, M. Synthesis of Fe_2O_3/TiO_2 nanorod-nanotube arrays by filling TiO_2 nanotubes with Fe. *Nanotechnology* **2008**, *19*, 315601. [CrossRef] [PubMed]
167. Yu, L.; Wang, Z.; Zhang, L.; Wu, H.B.; Lou, X.W.D. TiO_2 nanotube arrays grafted with Fe_2O_3 hollow nanorods as integrated electrodes for lithium-ion batteries. *J. Mater. Chem. A* **2013**, *1*, 122–127. [CrossRef]

168. Herrera, J.E.; Isimjan, T.T.; Abdullahi, I.; Ray, A.; Rohani, S. A novel nanoengineered VO_x catalyst supported on highly ordered TiO_2 nanotube arrays for partial oxidation reactions. *Appl. Catal. A Gen.* **2012**, *417*, 13–18. [CrossRef]
169. Guan, D.; Li, J.; Gao, X.; Yuan, C. Controllable synthesis of MoO_3-deposited TiO_2 nanotubes with enhanced lithium-ion intercalation performance. *J. Power Sources* **2014**, *246*, 305–312. [CrossRef]
170. Gobal, F.; Faraji, M. Fabrication of nanoporous nickel oxide by de-zincification of Zn–Ni/(TiO_2-nanotubes) for use in electrochemical supercapacitors. *Electrochim. Acta* **2013**, *100*, 133–139. [CrossRef]
171. Ortiz, G.F.; Hanzu, I.; Lavela, P.; Knauth, P.; Tirado, J.L.; Djenizian, T. Nanoarchitectured TiO_2/SnO_2: A future negative electrode for high power density Li-ion microbatteries. *Chem. Mater.* **2010**, *22*, 1926–1932. [CrossRef]
172. Wu, X.; Zhang, S.; Wang, L.; Du, Z.; Fang, H.; Ling, Y.; Huang, Z. Coaxial SnO_2@TiO_2 nanotube hybrids: From robust assembly strategies to potential application in Li^+ storage. *J. Mater. Chem.* **2012**, *22*, 11151–11158. [CrossRef]
173. Kim, M.; Lee, J.; Lee, S.; Seo, S.; Bae, C.; Shin, H. Nanotubular heterostructure of tin dioxide/titanium dioxide as a binder-free anode in lithium-ion batteries. *ChemSusChem* **2015**, *8*, 2363–2371. [CrossRef] [PubMed]
174. López, M.C.; Ortiz, G.F.; González, J.R.; Alcántara, R.; Tirado, J.L. Improving the Performance of Titania Nanotube Battery Materials by Surface Modification with Lithium Phosphate. *ACS Appl. Mater. Interfaces* **2014**, *6*, 5669–5678. [CrossRef] [PubMed]
175. Jha, H.; Hahn, R.; Schmuki, P. Ultrafast oxide nanotube formation on TiNb, TiZr and TiTa alloys by rapid breakdown anodization. *Electrochim. Acta* **2010**, *55*, 8883–8887. [CrossRef]
176. Allam, N.K.; Poncheri, A.J.; El-Sayed, M.A. Vertically oriented Ti-Pd mixed oxynitride nanotube arrays for enhanced photoelectrochemical water splitting. *ACS Nano* **2011**, *5*, 5056–5066. [CrossRef] [PubMed]
177. Kim, J.-Y.; Lee, K.-H.; Shin, J.; Park, S.H.; Kang, J.S.; Han, K.S.; Sung, M.M.; Pinna, N.; Sung, Y.-E. Highly ordered and vertically oriented TiO_2/Al_2O_3 nanotube electrodes for application in dye-sensitized solar cells. *Nanotechnology* **2014**, *25*, 504003. [CrossRef] [PubMed]
178. Oliveira, N.T.C.; Verdério, J.F.; Bolfarini, C. Obtaining self-organized nanotubes on biomedical Ti–Mo alloys. *Electrochem. Commun.* **2013**, *35*, 139–141. [CrossRef]
179. Yang, Y.; Kim, D.; Yang, M.; Schmuki, P. Vertically aligned mixed V_2O_5-TiO_2 nanotube arrays for supercapacitor applications. *Chem. Commun.* **2011**, *47*, 7746–7748. [CrossRef] [PubMed]
180. Paramasivam, I.; Nah, Y.C.; Das, C.; Shrestha, N.K.; Schmuki, P. WO_3/TiO_2 nanotubes with strongly enhanced photocatalytic activity. *Chem. Eur. J.* **2010**, *16*, 8993–8997. [CrossRef] [PubMed]
181. Raja, K.S.; Misra, M. Ordered Arrays of Ti-Mn Oxide Nanotubes for High Capacity Li-ion Battery. *ECS Trans.* **2011**, *33*, 31–44. [CrossRef]
182. Kim, J.H.; Zhu, K.; Yan, Y.; Perkins, C.L.; Frank, A.J. Microstructure and pseudocapacitive properties of electrodes constructed of oriented NiO-TiO_2 nanotube arrays. *Nano Lett.* **2010**, *10*, 4099–4104. [CrossRef] [PubMed]
183. Allam, N.K.; Deyab, N.M.; Ghany, N.A. Ternary Ti-Mo-Ni mixed oxide nanotube arrays as photoanode materials for efficient solar hydrogen production. *Phys. Chem. Chem. Phys.* **2013**, *15*, 12274–12282. [CrossRef] [PubMed]
184. Filova, E.; Fojt, J.; Kryslova, M.; Moravec, H.; Joska, L.; Bacakova, L. The diameter of nanotubes formed on Ti-6Al-4V alloy controls the adhesion and differentiation of Saos-2 cells. *Int. J. Nanomed.* **2015**, *10*, 7145–7163. [CrossRef] [PubMed]
185. Yang, M.; Yang, G.; Spiecker, E.; Lee, K.; Schmuki, P. Ordered "superlattice" TiO_2/Nb_2O_5 nanotube arrays with improved ion insertion stability. *Chem. Commun.* **2013**, *49*, 460–462. [CrossRef] [PubMed]
186. Madian, M.; Klose, M.; Jaumann, T.; Gebert, A.; Oswald, S.; Ismail, N.; Eychmüller, A.; Eckert, J.; Giebeler, L. Anodically fabricated TiO_2–SnO_2 nanotubes and their application in lithium ion batteries. *J. Mater. Chem. A* **2016**, *2*, 5542–5552. [CrossRef]

© 2018 by the authors. Licensee MDPI, Basel, Switzerland. This article is an open access article distributed under the terms and conditions of the Creative Commons Attribution (CC BY) license (http://creativecommons.org/licenses/by/4.0/).